2003

Voltammetric Study of Interaction of Copper and Model Fungal Secreted Ligands

Ran Liu
University of Maine - Main

VOLTAMMETRIC STUDY OF INTERACTION OF COPPER AND MODEL FUNGAL SECRETED LIGANDS

By

Ran Liu

B.E. Harbin Engineering University, 1997

A THESIS

Submitted in Partial Fulfillment of the

Requirements for the Degree of

Master of Science

(in Civil Engineering)

The Graduate School

The University of Maine

August, 2003

Advisory Committee:

Aria Amirbahman, Assistant Professor of Environmental Engineering, Co-Advisor

Barry Goodell, Professor of Wood Science and Technology, Co-Advisor

Jody Jellison, Professor of Molecular Plant Pathology

ACKNOWLEDGEMENTS

I wish to thank the University of Maine, Wood Utilization Research grant funds and the University Graduate Research Assistantship for making this research possible.

I would like to express my sincere gratitude to my advisors, Dr. Aria Amirbahman and Dr. Barry Goodell, for their guidance, encouragement and support throughout my graduate study. I would also like to thank my other committee member, Dr. Jody Jellison for her valuable comments, suggestions and supports during the past two years.

I wish to thank Mr. Yuhui Qian for his kindness and supports through the project.

My special gratitude goes to my husband Peng Chen and my parents – they are always there for me.

TABLE OF CONTENTS

LIST OF TABLES

LIST OF FIGURES

CHAPTER 1

INTRODUCTION

1.1 Background

Biodeterioration is a prime cause of failure of wooden structures in service and causes billions of dollars in loss every year. Conventional methods to prevent wood deterioration include the use of pressure systems to force preservative chemicals such as creosote or water-borne chromated copper arsenate into wood. However, environmental concerns require that new approaches and the use of more environmentally acceptable chemicals be found to prevent wood deterioration in a more appropriate manner. In order to develop environmentally acceptable methods to prevent wood decay, a better understanding of wood decay mechanisms is needed.

Brown rot fungi are some of the most important wood-degrading organisms[1]. They are characterized by their extensive and rapid depolymerization of cellulose leading to a rapid loss in wood strength at early stages of the decay process[2]. The mechanisms of wood degradation by brown-rot have been studied for decades, but to a less degree than that of white-rot fungi. It is believed that the decay process by brown-rot occurs by an initial non-enzymatic process, and that it involves a Fenton type catalytic system that produces hydroxyl radicals capable of attacking wood components[3-5].

Low molecular weight compounds produced by brown rot fungi have been proposed to mediate the redox cycling of iron to generate Fe(II), which reacts with H_2O_2 to produce highly reactive hydroxyl radicals. A study using the model chelator, 2,3-dihydroxybenzoic acid (2,3-DHBA), showed that this ligand not only has a high affinity

for binding Fe(III) but also will reduce Fe(III) to Fe(II)[5]. Recent research[6-8] has confirmed that compounds isolated from brown rot fungus *Gloeophyllum trabeum* will reduce Fe(III) to Fe(II), while, in the presence of quinone reductase enzymes, undergoing a quinone redox cycle to generate extracellular H_2O_2. However, quinone reductase enzymes have to great a molecular mass to penetrate the wood cell wall structure and this would limit this mechanism in decay progression.

Thus, study of the interaction between metals and low molecular weight compounds secreted by brown rot fungi will help us to gain a better understanding of the brown-rot decay mechanisms. In this thesis a voltammetric study of the interaction between Cu and two model fungal-secreted ligands (2,5-DMBQ and 2,3-DHBA) was conducted. Although Fe(III) has been the only transition metal hypothesized to function in the non-enzymatic Fenton based degradation system, this metal has a relatively low solubility even at low pH, and therefore Cu(II) was used as a model transition metal in this work. Cu also undergoes Fenton type reactions with H_2O_2 to produce hydroxyl radicals.

1.2 Scope and objectives of study

The general objective of this research is to study the interaction between metals and the low molecular weight chelators isolated from *G. trabeum*, from which a better understanding of nonenzymatic wood decay process by brown rot fungi can be obtained.

The binding capacity of 2,5-dimethoxybenzoquinone (2,5-DMBQ, one of low molecular weight chelators secreted by *G. trabeum*) with Cu will be studied by using CLE/ASV (competitive ligand exchange/ anodic stripping voltammetry) method, from which the stability constants between 2,5-DMBQ and Cu can be determined. The stability

constant for Cu and 2,5-DMBQ will be useful for comparing the affinity of this quinone to other ligands in the decay environment and could help explain a possible mechanism for the non-enzymatic quinone redox cycle hypothesized to exist in brown rot wood decay processes.

In addition, the reaction characteristics of Cu and 2,3-DHBA (a model ligand for Gt chelators) will be studied by the cyclic voltammetry method. The cyclic voltammetry data will provide information on the thermodynamics of the redox processes and will be useful for identification of redox potentials of the electroactive species, and evaluation of the effect of environmental conditions upon the redox process. The cyclic voltammetric study of the interaction between Cu and 2,3-DHBA in the absence and presence of H_2O_2 will help to improve our understanding of reaction mechanisms related to a Fenton-type catalytic system proposed to be involved in wood decay processes.

1.3 Thesis organization

This thesis is divided into five chapters. The background and objectives are presented in chapter one. Chapter two discusses the current understanding of brown-rot decay mechanisms and the theories and advantages of the CLE/ASV method and cyclic voltammetry method in this research. In chapter three, the CLE/ASV and cyclic voltammetry methods are described. Chapter four presents the results of the experiments and the related discussion. Chapter five presents a summary and conclusions of the work, along with suggestions for future work.

CHAPTER 2

LITERATURE REVIEW

2.1 Introduction

Brown rot decay is the most common and most destructive type of decay in Northern Hemisphere forests and in structural wood products. It causes billions of dollars in loss each year in the United States and the rest of the world[9]. To effectively prevent wood decay in an environmentally appropriate manner, a systematic understanding of the mechanisms of wood biodegradation by brown rot fungi is needed.

The wood decay mechanisms used by brown rot fungi have been previously hypothesized to involve a non-enzymatic pathway[10]. In particular, this pathway has been proposed to include a free radical mechanism initiated by the reduction of metals such as Fe or potentially other transition metals by the low molecular weight organic compounds produced by brown rot fungi in the early stages of wood degradation[5, 11]. Most of the work supporting this hypothesis has been based on the activity of Gt chelators that have been isolated from the brown rot fungus *Gloeophyllum trabeum*. Recently, three compounds, 4,5-dimethoxycatechol (4,5-DMC), 2,5-dimethoxyhydroquinone (4,5-DMBQ) and 2,5-dimethoxybezonquinone (2,5-DMBQ), have been isolated from the brown rot fungus *G. trabeum* and a related study indicated that these compounds have the ability to reduce Fe (III) and to initiate an extracellular Fenton reaction in brown rot wood degradation processes[6-8].

2.2 Mechanisms of wood degradation by brown rot fungi

The mechanisms and hypotheses involved in non-enzymatic free radical production in brown rot fungi are presented in this section. Most published research concerning the activity of Gt chelators has dealt with the binding of Fe by these ligands or by model ligands such as 2,3-DHBA.

2.2.1 Non-enzymatic wood decay mechanisms

The most serious kind of microbiological deterioration of wood is caused by fungi because some types of wood degrading fungi can cause rapid structural failure. Brown rot fungi are characterized by their ability to degrade the cellulose and hemicellulose of the wood cell wall rapidly and selectively, leaving the lignin modified but unmetabolized [12]. Historically, this was considered as a purely enzymatic process [13]. Later research [9], however, revealed that degradation was not localized near the hyphae of fungi, as even the smallest fungal extracellular enzymes are too large to penetrate the wood cell wall and reach cellulose in early decay stages[14, 15]. Instead, the low molecular weight compounds produced by brown rot fungi were hypothesized to be capable of diffusing into the wood cell wall to initiate the decay process. This suggested the degradation of cellulose by brown-rot fungi must involve a non-enzymatic process at least in the initial stages of degradation.

Halliwell[10] first proposed the possibility of the existence of a non-enzymatic cellulolytic system involving peroxide and iron based on the observation of the degradation of cotton cellulose by Fenton's reagent (H_2O_2/Fe^{2+}). Subsequently, Koenigs[3, 4] demonstrated that cellulose in wood can be depolymerized by Fenton's reagent, that

brown-rot fungi produce extracellular H_2O_2, and that wood contains enough iron to make Halliwell's hypothesis viable[16]. The production of hydroxyl radicals ($OH^{\bullet}$) from Fe^{2+} and H_2O_2 by the Fenton reaction [2, 17] is shown as:

$$Fe^{2+} + H_2O_2 \rightarrow Fe^{3+} + OH^- + OH^{\bullet} \quad (2\text{-}1)$$

The hydroxyl radicals produced by the above Fenton reaction were proposed to cleave long chain cellulose molecules into small fragments. Given the very short half life of $OH^{\bullet}$, this species does not diffuse into wood, and as such, it has been argued that it must be formed at its site of reaction[5]. Further research in this area by Highley[18] and Schmidt et al.[2] showed that wood degraded by reactive products of the Fenton reaction displayed the unique features similar to that of brown rotted wood. All this research suggests that brown rot decay involves a Fenton-type catalytic system that produces $OH^{\bullet}$ to attack and degrade wood components. But a plausible explanation for the sources of the requisite Fe(II) and H_2O_2 in above reaction schemes was needed to fulfill the non-enzymatic decay process.

2.2.2 Hypotheses on the source of Fenton reagents

Several hypotheses have been recently proposed for the source of Fenton reagents in the brown rot decay process. Hyde and Wood[19] suggested that the decay process involves the reduction of Fe(III) by cellobiose dehydrogenase (CDH) within the fungal cells, diffusion of the produced Fe(II) away from the hyphae, formation of an Fe(II)-oxalate complex, and finally, hydroxyl radical formation at a safe distance from the hyphae. But a weak point of this model is the very slow interaction of CDH with Fe(III)[6].

Enoki et al.[20, 21] postulated that Fe(III) is coordinated to a glycopetide and the presence of extracellular NADH (nicotinamide ademine dinucleotide) or ascorbate is required to reduce Fe(III). However, no evidence was presented to suggest that NADH is secreted outside the cells of brown-rot fungi[6].

Shimada et al.[22] proposed that brown rot fungi might use oxalic acid as a chelator and a reductant for an Fe(II)-H_2O_2 system to generate hydroxyl radicals. However, oxalate does not reduce Fe(III) except as a light-dependent reaction[19, 23, 24]. Therefore, oxalate cannot function as a direct catalyst of Fenton type chemical reaction in wood, where light levels are low.

Goodell et al.[5] proposed that a low molecular weight metal chelator other than oxalate is involved in brown rot wood decay. Their model suggested that the natural chelators produced by brown rot fungi not only have a strong affinity for Fe(III) but also mediate redox cycling of iron at the low pHs associated with fungal cultures. Fe(II) produced from the reduction of Fe(III) by the low molecular weight chelators could then react with H_2O_2 to produce reactive oxygen species involved in the wood brown rot decay process. This model is illustrated in Figure 2.1.

In this model, the Gt chelators (with ortho-dihydroxy substituted benzoic compounds as the primary components) can diffuse into the wood cell wall where they bind metals to initiate redox cycling reactions. The reduced metals then react with hydrogen peroxide, which is produced either directly from the fungus, or from the oxidation of semiquinones and other phenolic compounds that can be formed from Gt chelators. These reactions produce reactive oxygen species such as $OH^{\bullet}$ and peroxyl radicals ($HOO^{\bullet}$ and O_2^{-})[25] that would degrade cellulose and hemicellulose. Further

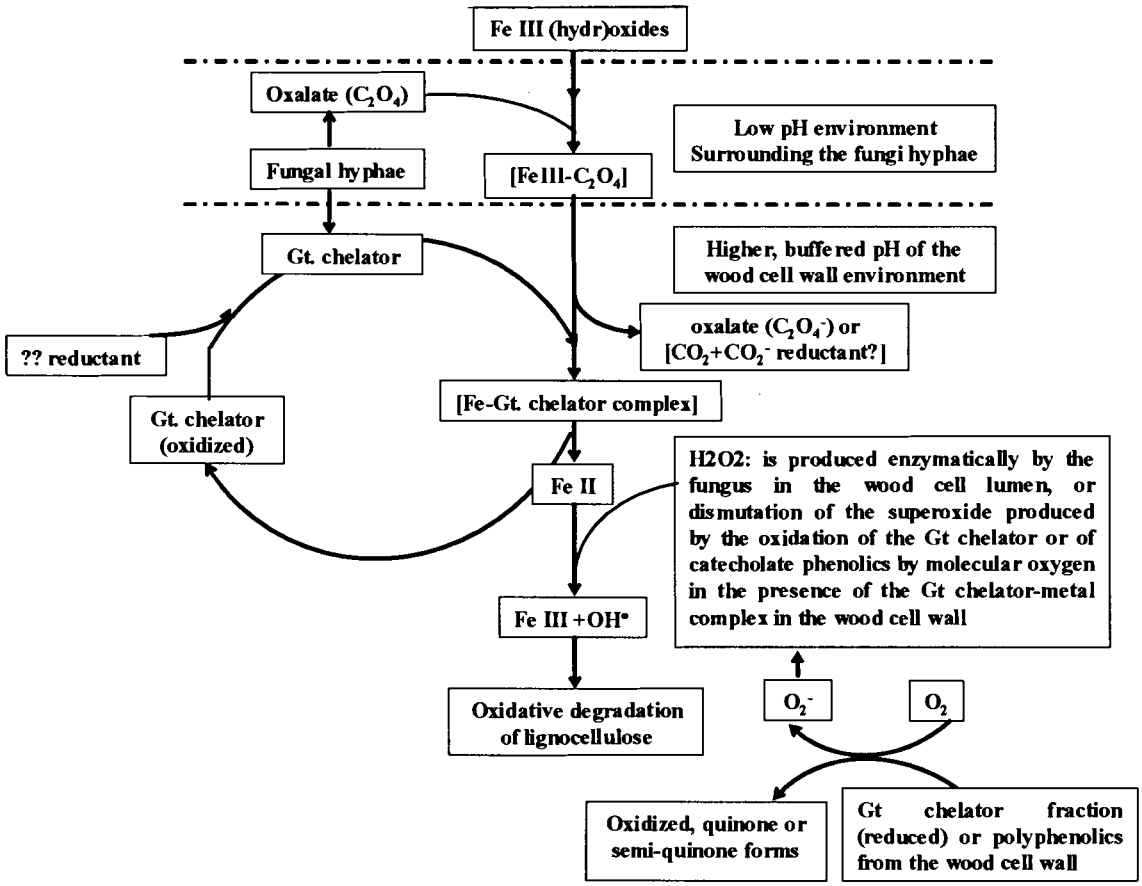

Figure 2.1: Proposed mechanism for Gt. chelator mediated degradation of wood by the fungus *Gloeophyllum trabeum* (Goodell et al., 1997)

research is required to explore the mechanism of chelator redox cycling within the wood cell wall to substantiate this model.

Wang and Gao[26, 27] also proposed that a special low-molecular-weight peptide named Gt factor has a high affinity of chelating with Fe^{3+} and could reduce Fe^{3+} to Fe^{2+}. Their work demonstrated that the Gt factor could mediate the formation of hydroxyl radical $OH^{\bullet}$ and play an important role in the initial degradation of lignocellulose.

2.2.3 Studies on the low molecular weight fungal chelators

Low molecular weight chelators were first isolated from white and brown rot fungi in the late 1980's and early 1990's[28, 29]. Isolated chelators from the brown rot fungus *Gloeophyllum trabeum* have small molecular size (<1000 dalton), allowing them, unlike enzymes, to penetrate through the wood cell wall matrix[30] where they could mediate redox reactions to generate hydroxyl and superoxide radicals[31]. However, the availability of iron in wood is limited [32]. Iron in the wood may not exist as a free cation but be bound to the wood cellulose or in hydr(oxide) form[33, 34]. Research has revealed that oxalate in the wood may sequester water insoluble Fe(III) and solubilize it, making it available for reaction with the Gt chelator[5]. The work of Xu and Goodell[34] also suggested that oxalate and Gt chelator secreted by brown rot fungi are capable of diffusing into the wood cell wall to sequester Fe(III) from cellulose to form oxalate-iron complexes and Gt chelator-iron complexes, and to initiate the redox cycling within the wood cell wall.

More recent work has focused on the redox cycling pathways of iron and Gt chelators. Paszczynski et al.[6] identified two compounds, 4,5-dimthoxy-1,2-benzenediol

(DMC) and 2,5-dimethoxy-1,4-benzenediol (DMH), in the Gt chelator. DMC and DMH are interesting compounds in that the methoxyl groups increase redox reactivity of the hydroxyls, which can readily reduce oxygen. Jensen et al.[8] also reported that DMC and DMH are able to rapidly reduce Fe(III) even in the presence of oxalate at pH 4. Since DMC was found both extracellularly and within the fungal cells[6], it is a good candidate for an electron carrier between hyphae and Fenton reaction centers outside the cell. Also, DMC and DMH in their quinone forms could be involved in the redox reactions during brown rot fungi decay process. Kerem et al.[7] confirmed the presence of DMH in the culture medium of *G. trabeum*, and also reported the presence of 2,5-dimethoxy-1,4-benzoquinone (DMBQ) in the same culture medium. Their work also demonstrated that *G. trabeum* can use a quinone redox cycle to generate extracellular Fe^{2+} and H_2O_2, the two ingredients needed for Fenton chemistry (Figure 2.2). However, it is unlikely that this reaction occurs as part of the wood degradation process because the required quinone reductase enzyme, like all enzymes, is too large to penetrate the intact wood cell wall. The mechanism proposed would require an active redox cycling system deep within the wood cell wall layers. Other researchers[7, 35] showed that there are quinone reductases produced by *G. trabeum* capable of eliciting high levels of extracellular quinone redox cycling, but it is not clear what the function of these enzymes have. Goodell et al.[36] and Qian and Goodell[37] have shown that repeated iron reduction can occur in the presence of catechol and iron alone, without enzymatic activity. The mechanism for this is presumed to be the oxidation of catechol or its breakdown products, but more study on this is needed. DMC and DMH appear to fit well into the model of brown rot decay proposed by Goodell et al.[5], however, the mechanism for the iron cycling is as yet unknown.

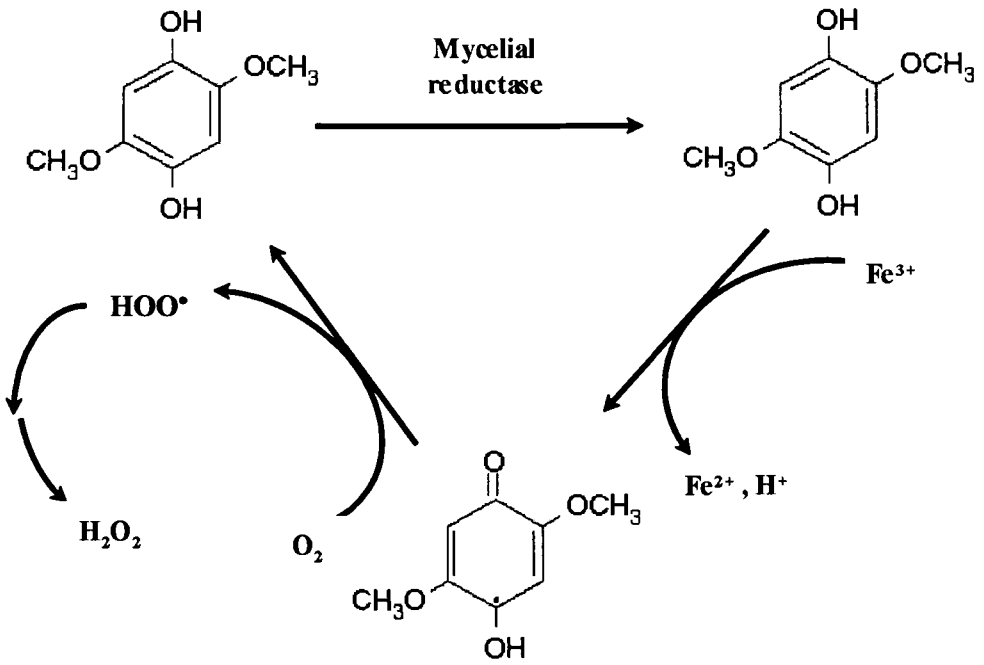

Figure 2.2: Proposed pathway for extracellular Fe^{3+} reduction and H_2O_2 production by *G. trabeum* (Kerem, et al., 1999)

It is unclear how these chelating compounds (DMC, DMH and DMBQ) compete with other metal complexes such as oxalate to sequester and reduce iron to initiate quinone redox cycling. In this work, the binding characteristics of DMBQ and Cu will be examined by competitive ligand exchange/ anodic stripping voltammetry (CLE/ASV) method. This will give a trend of binding affinity between iron and these compounds and help to improve understanding of the biochemical processes employed by brown rot fungi.

2.3 Metal–ligand complexation using CLE/ASV

2.3.1 Metal speciation

Metal ions occur in natural waters or aquatic environments in a variety of chemical forms, namely as free aquo ions, as complexes with inorganic and organic ligands, as particulate (or colloidal) phases, and adsorbed on particulate (or colloidal) phases[38] . These different chemical species have different degrees of reactivity and availability. The availability of metal ions to organisms, as well as their toxic effects, strongly depends on chemical speciation[39]. In many instances the effects have been shown to be related to the concentration of free aquo ions[40], which is regulated by complex interactions between various ligands in solution, particle surface and biota. In order to evaluate the fate and effects of metal ions in natural environments, it is thus essential to understand their speciation.

2.3.2 Anodic stripping voltammetry

Anodic stripping voltammetry (ASV) has been widely used for metal speciation studies[41]. It involves the electrochemical preconcentration of reducible species,

primarily metallic ions, from a solution containing trace quantities of such analytes onto the surface of an electrode. This step is followed by the application of a potential ramp in the anodic direction, generating a current that results from the oxidation of the preconcentration analyte(s) on the electrode surface. ASV has good sensitivity (down to nanomolar concentrations) and distinguishes between labile and non-labile species. The labile species are reducible at the specific deposition potential on the time scale of the electrochemical method; they include inorganic species (free aquo ions and inorganic complexes) and readily dissociable weak organic complexes. The difference between the total and labile species is called the non-labile (inert) species. Even though ASV does not directly determine the concentration of free metal ions[42], it is still a useful method for speciation because of its sensitivity and ability to distinguish labile metal species from strong organic complexes, as well as those species bound to the particulate phase[43].

Differential pulse anodic stripping voltammetry (DPASV) is the most widely used ASV technique. The application of this technique often involves titration of natural water with metal ions, from which the stability constants of metal-organic complexes and ligand concentrations can be obtained[44].

The ASV technique was used in the current research to help determine the type (labile or inert) species of Cu binding with the model hydroquinone. The importance of this understanding was to allow a determination of the stability constants between Cu and 2,5-DMBQ by choosing an appropriately competitive ligand. After determining the stability constant of Cu-2,5-DMBQ complexes, the binding affinity can be compared with that of Cu and other organic ligands, such as oxalic acid in the wood decay

environment. Thus, a better understanding of the brown rot decay mechanisms involved in the interaction between metals and fungal secreted ligands will be obtained.

2.3.3 Competitive ligand-exchange technique

Ligand-exchange techniques are based on the competition between natural ligands and added known ligands for metals, and the subsequent specific and sensitive measurement of the affinity of these known ligands for the metals. The free metal ion concentrations are then determined by equilibrium calculations, on the basis of the concentration of complexes formed with the known ligands, and their stability constants.

A variety of organic ligands, such as EDTA, ethylenediamine, catechol, hydroxyquinoline and tropolone have been used as exchanging ligands to determine the stability constants for metal-organic complexes[38]. Ligand-exchange anodic stripping voltammetry with added ethylenediamine as the labile ligand has been used to study the binding of Cu with dissolved organic matter in seawater[45]. Cathodic stripping voltammetry of labile Cu-catechol complexes was used for Cu speciation in the presence of natural organic matter in Altantic seawater[46], in estuarine water[47] and in lake water[48, 49]. Beside copper, the speciation of many other metals including several transition metals may also be determined with stripping voltammetry and various competitive ligand-exchange techniques[50-52]. All of the aforementioned studies used the competitive ligand-exchange method combined with stripping voltammetry techniques to estimate the thermodynamic stability constants of metal and natural organic ligands, such as humic substances[53-55].

The ligand-exchange followed by voltammetric measurements, DPASV or DPCSV, has shown advantages with good sensitivity and without pre-separation. With ligand competition techniques, the detection of unknown ligands depends on the values of the complexing coefficient of added competing ligands (α-value, production of stability constant times free ligand concentration) and also on analytical sensitivity[38].

2.4 Cyclic voltammetry methods

2.4.1 Theory

Cyclic voltammetry is a widely used technique for acquiring qualitative information about electrochemical reactions. The power of cyclic voltammetry results from its ability to rapidly provide considerable information on the thermodynamics of redox processes, on the kinetics of heterogeneous electron-transfer reactions and on coupled chemical reactions or adsorption processes[56]. In particular, this technique offers rapid identification of redox potentials of the electroactive species, and convenient evaluation of the effect of environmental parameters upon the redox process.

Cyclic voltammetry is done by linearly scanning the potential of a stationary working electrode (in an unstirred solution) using a triangular potential waveform (Figure 2.3). Depending on the information sought, single or multiple cycles can be used. During the potential sweep, the potentiostat measures the current resulting from the applied potential. The resulting plot of current versus potential is termed a cyclic voltammogram. The cyclic voltammogram is a complicated, time-dependent function of a large number of physical and chemical parameters.

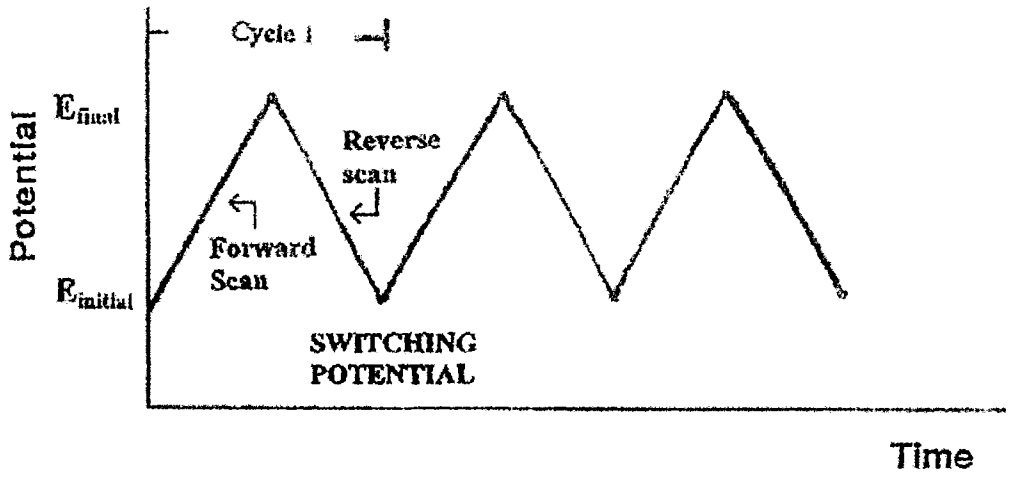

Figure 2.3: Potential-time excitation signal in cyclic voltammetric experiment (Wang, 2000).

Figure 2.4 illustrates the response of a reversible redox couple during a single potential cycle. It is assumed that only the oxidized form "O" is present initially. Thus, a negatively directed potential scan is chosen for the first half cycle, starting from a value where no reduction occurs. As the applied potential approaches the characteristic E^0 for the redox process, a cathodic current begins to increase, until a peak is reached. After traversing the potential region in which the reduction process takes place, the direction of the potential sweep is reversed. During the reverse scan, the reduced "R" molecules (generated in the forward half cycle, and accumulated near the surface) are reoxidized back to "O" and an anodic peak results.

For a reversible electrochemical reaction, the cyclic voltammogram recorded has certain well-defined characteristics:

1) The voltage separation between the current peak is:

$$\Delta E = E_p^a - E_p^c = \frac{0.059}{n} V \qquad (2\text{-}2)$$

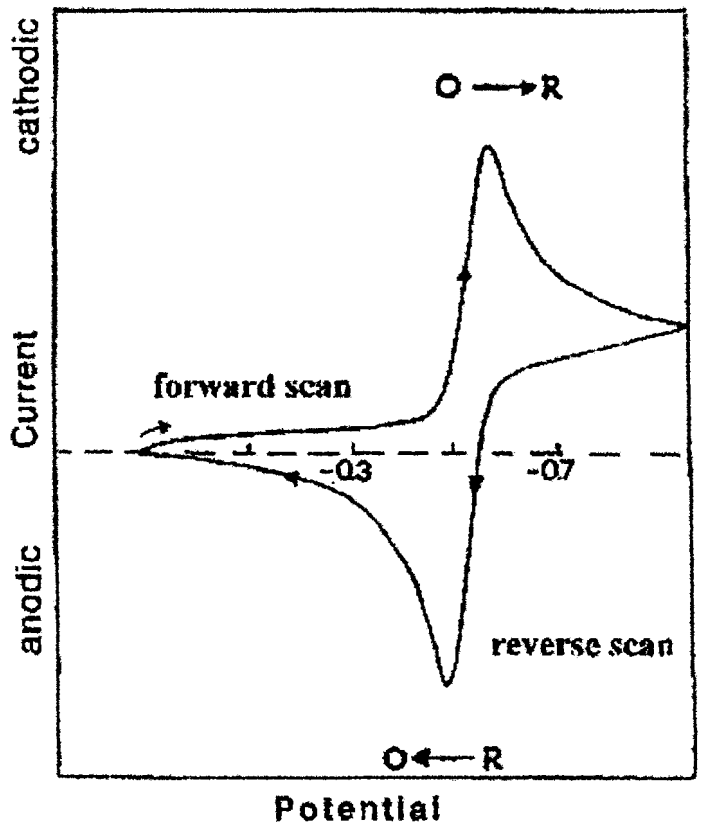

Figure 2.4: Typical cyclic voltammetry for a reversible O + ne$^-$ ⇔ R redox process (Wang, 2000).

where n is the number of the electrons transferred during the redox process.

2) Neither the cathodic and anodic peak potentials alter as a function of voltage scan rate.

3) The ratio of the peak currents is equal to one:

$$\left|\frac{i_p{}^a}{i_p{}^c}\right| = 1 \qquad (2\text{-}3)$$

4) The peak currents are proportional to the square root of the scan rate v,

$$i_p{}^a \text{ and } i_p{}^c \propto \sqrt{v} \qquad (2\text{-}4)$$

The influence of the voltage scan rate on the current for a reversible electron transfer can be seen in Figure 2.5. Each curve has the same form but the total current increases with increasing scan rate. This can be explained in terms of the diffusion layer thickness. The cyclic sweep voltammogram will take longer to record as the scan rate is decreased. Therefore, the size of the diffusion layer about the electrode surface will be different depending upon the voltage scan rate used. In a slow voltage scan, the diffusion layer will grow much further from the electrode in comparison to a fast scan. Consequently the flux to the electrode surface is considerably smaller at slow scan rates that it is at fast rates. As the current is proportional to the flux towards the electrode, the magnitude of the current will be lower at slow scan rates and higher at fast rates.

For the irreversible electron transfer process, the cyclic voltammogram shows a different behavior from its reversible counterpart. Figure 2.6 illustrates a series of voltammograms recorded at a single voltage sweep rate for a quasi-reversible reaction for different values of the reduction and oxidation rate constants.

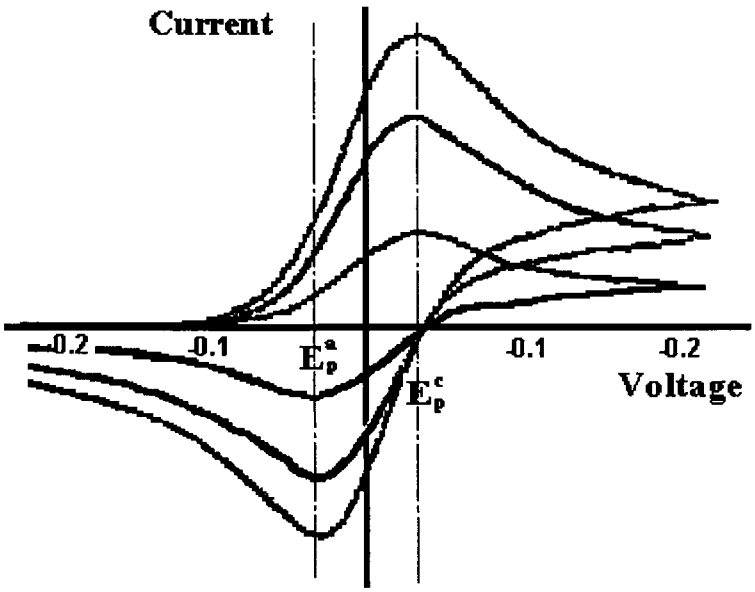

Figure 2.5: Current peak changes with scan rates for reversible electron transfer processes[57].

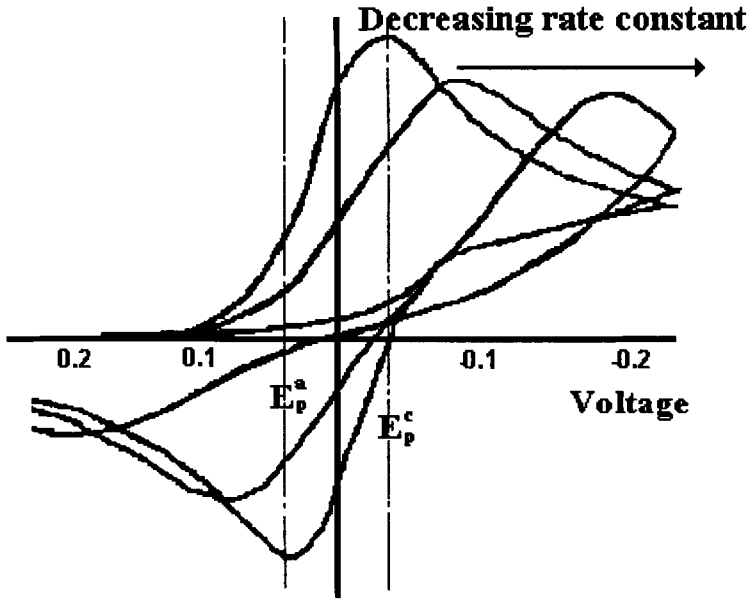

Figure 2.6: Current changes with different reduction and oxidation rate constants for irreversible electron transfer processes at a single voltage scan rate [57].

The first curve in Figure 2.6 shows the case where both the oxidation and reduction rate constants are still fast. The other two curves show the cases for lower rate constants but at the same scan rate. For decreasing rate constants, the curves shift to higher reductive potentials as shown in Figure 2.6. Again this can be explained in terms of the fact that equilibrium at the surface is no longer establishing so rapidly. In these cases, the peak separation is no longer fixed but varies as a function of the scan rate. Similarly, the peak current no longer varies as a function of the square root of the scan rate. By analyzing the variation of peak position as a function of scan rate, for reactions where a chemical reaction in solution is followed by an electron transfer step at the surface of the electrode, it is possible to gain an estimation of the electron transfer rate constants[58] .

2.4.2 CV application to the interaction between metals and hydroquinones

Cyclic voltammetry methods have been used to characterize the oxidation state and the type of binding between hydroquinones and metals ions in dimethyl sulfoxide (DMSO) solutions. Hatzipanayioti, et al.[59] studied the interactions between 2,3-dihydroxy-benzoic acid (2,3-DHBA) and Mn(II) in DMSO solution using cyclic voltammetry. They demonstrated that 2,3-DHBA is electrochemically oxidized to the dimeric semiquinone form by two one-electron transfer steps. Under anaerobic conditions, 2,3-DHBA formed stable complexes of the MnL_2 type with Mn(II) and Mn(III), while in the presence of air the oxidized forms of the ligand reacted with Mn(II) to give a mixed-valence species. Bodini et al.[60] used the same method to investigate 3,4-dihydroxy-2-benzoic acid (3,4-DHBA) interactions with Mn(II) and Mn(III). Their results showed that 3,4-DHBA is also oxidized to the semiquinone and quinone by two one-electron transfer

steps. The presence of a semiquinone dimer was formed by a stable complex with Mn(II) and Mn(III) was proposed. A similar approach will apply to the study the interaction 2,3-DHBA and Cu in this work.

In this work, if any effect on the electrochemical redox process of 2,3-DHBA by Cu(II) is found, it will help in characterizing the mechanism of the interaction between Cu and 2,3-DHBA. In the presence of H_2O_2, if an effect of H_2O_2 on the redox process of Cu and 2,3-DHBA is observed, it may indicate that Fenton type reactions can be affected by Cu and 2,3-DHBA as well as H_2O_2. Alternately, we may difference in redox potential of 2,3-DHBA that are affected by changes in pH. In this case, since the pH of the fungal/wood environment may change significantly within a mater of microns, and microsite pH values may range from 2.0 near the fungal hyphae to 6.0 within the wood cell wall, understanding how pH affects oxidation of 2,3-DHBA by Cu(II) can be important in understanding how this will affect decay processes. When these basic mechanisms are understood, they can be compared to the results obtained from Fenton chemistry studies involved in brown rot decay process in the literature. Thus, a better understanding the mechanism of Fenton type reactions involved in brown rot decay process can be obtained or developed.

CHAPTER 3

MATERIALS AND METHODS

3.1 Introduction

The experimental work here focuses on: 1) the development of the Competitive Ligand Exchange / Anodic Stripping Voltammetry (CLE/ASV) method to study the binding of Cu with low molecular organic acids (Gt chelators) secreted by brown rot fungus *Gloeophyllum trabeum* at a range of pHs, and 2) the study of the interaction between Cu and a model fungal-secreted ligand, 2,3-DHBA, using the cyclic voltammetry method.

3.2 Reagents and material preparation in this research

3.2.1 Labware cleaning

Deionized water was obtained from a NANOpure ultrapure water system. The source water was double distilled in house from a Mega-Pure distillation system.

Since a very low concentration of Cu was used in the CLE/ASV experiments, all the labware for storage solutions were meticulously cleaned with a 5M solution of trace grade HNO_3, and rinsed with D.I. water before use. The Teflon tubes used to synthesize the samples were cleaned with a 1% (v/v) solution of trace grade HNO_3 and rinsed with D.I. water before use. The Teflon vessel used in the voltammetry instrument was kept in a 0.1% (v/v) solution of trace grade HNO_3 when not in use, and rinsed with D.I. water before use.

3.2.2 Reagents for CLE/CSV experiments

The chemical solutions used in the CLE/ASV experiments were prepared as follows:

$CuCl_2$ stock solution at a concentration of 5×10^{-3} M was prepared by dissolving 0.0336g ACS analytical grade $CuCl_2$ in 50mL of trace grade 0.1M HCl. The solution was kept in a plastic bottle and was used within 2 weeks. 2,3-DHBA stock solution, 5×10^{-3} M, was made by dissolving 0.0385g 99.9% 2,3-DHBA in 50mL of double distilled deionized (D.I.) water. This solution was aerated with Argon gas to remove oxygen and was stored in a dark glass bottle. 2,5-DMBQ stock solution, 5×10^{-3} M, was made by dissolving 0.0425g 2,5-DMBQ in 50mL of 0.1M NaOH and was stored in a dark glass bottle. EDTA stock solution, 1×10^{-3} M, was made by dissolving 0.02922g ACS analytical grade EDTA in a 100mL of 0.02M NaOH and was stored in a dark glass bottle. KNO_3 solution, 1.5M, was made by dissolving 15.15g KNO3 in 100mL of D.I. water. To this solution, 0.1mM of MnO_2 was added to remove any iron that might be present in the background[61]. This solution was shaken for 8h followed by filtration through a 0.2μm syringe filter (GelmanSciences). Acetate buffer, 2 M pH 4, was prepared by dissolving 3.281g sodium acetate and 9.15mL 100% acetic acid in 100mL of D.I. water; 2M pH 5, was prepared by dissolving 11.550g sodium acetate and 3.83mL 100% acetic acid in 100mL of D.I. water. Phosphate buffer, 2M pH 6, was prepared by dissolving 25.94g sodium phosphate monobasic anhydrous (NaH_2PO_4) and 1.685g sodium phosphate dibasic salt (Na_2HPO_4) in 100mL of D.I. water. HEPES buffer, 1M pH 6.9, was prepared by dissolving 23.83g of HEPES in about a 100 ml flask and titrating it with 5M NaOH to pH 6.9. Except for 2,5-DMBQ, which was purchased from Tokyo Kasei Kogyo Co. LTD, all reagents were purchased from Sigma-Aldrich company.

3.2.3 Reagents for CV experiments

The 2,3-DHBA stock solution at a concentration of 0.05M was made by dissolving 0.77g 2,3-DHBA in 100mL of 0.025M NaOH. $CuCl_2$ stock solution, 0.5M, was made by dissolving 3.36g $CuCl_2$ in 50mL of 0.01M HCl. KNO_3 solution, 1.5M, was prepared and purified as described in section 3.2.7. H_2O_2 solution, 0.185M, was made by diluting 1mL of 30% (w/w) H_2O_2 solution in 49mL of D.I. water. NaOH solution, 0.05M, was made by dissolving 20g sodium hydroxide in 100mL of D.I. water to 5M solution, which is diluted 100 times by adding proper amount of D.I. water. HCl solution, 0.05M, was made by diluting 425μL 37% HCl in 100mL of D.I. water. 0.05M NaOH and HCl solutions were used to adjust the pH of the analytes. All the reagents were purchased from Sigma-Aldrich.

3.3 CLE/ASV method

3.3.1 General approach

The CLE/ASV method presented here for the determination of Cu complexation by low molecular weight organic ligands is based on the competition between natural organic ligands and the added ligands, and the Differential Pulse Anodic Stripping Voltammetry (DPASV) measurement. A similar approach was also used by Xue and Sigg[48] when studying the binding of copper to organic lignands in lake water. Using DPASV, a distinction is made between electrochemically labile and inert species. The inert Cu species are the complexes that are not dissociated in the boundary layer of the mercury electrode at the specific deposition potential within the electrochemical time

scale, and that are not reduced. The labile species are electroreactive and can be reduced on the mercury electrode and give a current peak at a certain potential.

Using the competitive ligand exchange approach, a ligand whose complexation equilibria with Cu are well characterized is added to compete with a ligand of unknown binding characteristics. The added ligand must be inert if the studied ligand is labile, or it must be labile if the studied ligand is inert. For a given total concentration of Cu, by varying the ratio of Cu, the studied ligand and the added ligand, the concentration of Cu complexing with the studied ligand can be determined, and the stability constants for the interaction between Cu and the studied ligand can be calculated.

3.3.2 Selection of the competing ligand

Two organic ligands, 2,3-dihydroxybenzioc acid (2,3-DHBA) and 2,5-dimethoxybenzoquinone were studied using the CLE/ASV method. Preliminary experimental results indicated that Cu complexes of both 2,3-DHBA and 2,5-DMBQ are fully labile ligands in an aqueous acidic solution. Therefore, an inert ligand was needed as the competing ligand.

Ethylenediaminetetraacetic acid (EDTA) was chosen here as an inert ligand to compete with 2,3-DHBA or 2,5-DMBQ. The concentration of DPASV labile Cu was followed as a function of added EDTA. The concentration of CuEDTA complexes formed was calculated from the difference between initially labile Cu and labile Cu after addition of EDTA, from which the stability constants for Cu and 2,3-DHBA or 2,5-DHBA were calculated. The concentration of EDTA used in a sample solution was

chosen to allow approximately 20% to 80% of total Cu bind with EDTA to prevent errors due to very low or high Cu binding.

3.3.3 Determination of the working limit for DPASV

The detection limit for Cu using the stripping voltammetry technique can reach down to picomolar levels. However, this requires a very clean experimental environment and very pure reagents. In our experiments, the total concentration of Cu used in all the CLE/ASV experiments was between 5×10^{-9} M and 5×10^{-6} M, which is low enough to simulate natural wood decay conditions. Preliminary experiments indicated that 5×10^{-5} M 2,3-DHBA or 3×10^{-5} M 2,5-DMBQ are suitable to obtain a good calibration curve of Cu-labile ligand complexes by CLE/ASV.

3.3.4 Voltammetric instrument

The voltammetric measurement system consisted of a hanging mercury drop electrode (HMDE), an Ag/AgCl, KCl (saturated) reference electrode and a platinum auxiliary electrode held in a Metrohm 747 VA stand, and a Metrohm 746 VA trace analyzer which connected with a PC for data storage and processing. The Metrohm 746 VA trace analyzer controls the 747 VA stand via a set-up procedure for the voltammetric measurement and records the resulting DPASV curves.

The voltammetric experiments were conducted in a Teflon vessel. The three electrode system of the 747 VA stand is illustrated as below in Figure 3.1:

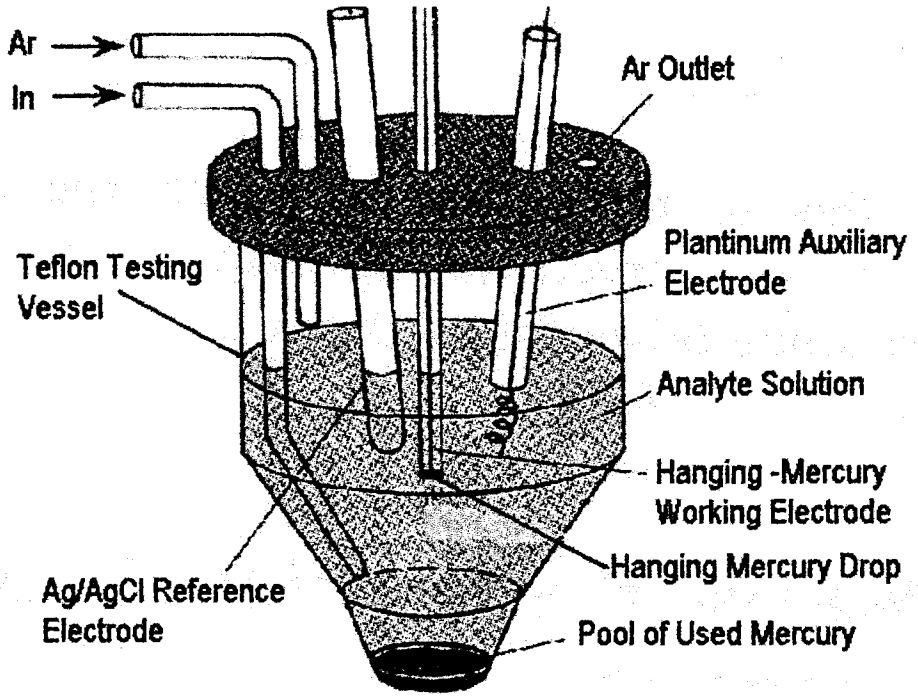

Figure 3.1: The three electrode working system of the Voltammetric instrument.

3.3.5 CLE/ASV experimental procedure

3.3.5.1 Phase I: Cu-2,3-DHBA-EDTA system

2,3-DHBA was used initially as a model ligand for the Gt. chelator to examine whether the CLE/ASV method was feasible for the study of the binding of Cu with organic ligands under acidic conditions. The experimental results of Cu-2,3-DHBA complexes were then compared with the model predicted values.

3.3.5.1.1 Sample solutions

Two sets of solutions for the study of Cu-2,3-DHBA binding were synthesized in acid washed Teflon tubes. One set contained 5×10^{-9} M to 5×10^{-6} M $CuCl_2$, 5×10^{-5} M 2,3-

DHBA, 0.01M KNO_3 and 0.03M buffer (for pH 4 and 5, acetate buffer was used; for pH 6.9, HEPES buffer was used). The other set of solutions contained the same amount of the above reagents plus 5×10^{-9} M EDTA for Cu concentrations from 5×10^{-9} M to 1×10^{-7} M, and 1×10^{-7} M EDTA for Cu concentrations from 1×10^{-7} M to 5×10^{-6} M. All the samples were placed in an incubator at 22 °C and rotary shaken in the dark overnight before the DPASV measurement.

3.3.5.1.2 DPASV measurements of Cu-2,3-DHBA complexes

Prior to the start of the experiment, the sample solution was added in the Teflon vessel, then stirred and bubbled with Suprapure Argon for 3min. A hanging mercury drop was then formed at the working electrode to allow the deposition of all species including the Cu-2,3-DHBA complexes at the mercury drop. One minute was deemed sufficient for the deposition of species at the electrode surface with an applied potential of –200mV. After the deposition period, the stirrer was turned off. After 15 sec, the voltage scan was started in the positive direction. Scanning parameters were: initial potential of –600mV, ending potential of 300mV (vs. Ag/AgCl reference electrode), pulse height of 50mV, and scan rate of 50mV/s. DPASV measurements were carried out at room temperature about 20 °C. The oxidation peak potential of all the labile Cu species, including Cu-2,3-DHBA complexes, was between –100mV and +50mV depending on the pH. The height of current peak was proportional to the concentration of the labile Cu species in the sample solution. This peak decreased when EDTA was added due to the formation of non-labile Cu-EDTA complexes.

3.3.5.2 Phase II: Cu-2,5-DMBQ-EDTA system

3.3.5.2.1 Sample solutions

As above in section 3.2.5.1.1, two sets of solutions, one with EDTA and one without EDTA were prepared. One set contained 5×10^{-8} M to 1×10^{-6} M $CuCl_2$, 2.5×10^{-5} M 2,5-DMBQ at pH 4 and 3×10^{-5} M 2,5-DMBQ at pH 5 and 6, 0.12M KNO_3 and 0.03M buffer (for pH 4 and 5, acetate buffer was used; for pH 6, phosphate buffer was used). The other set contained the same amount of above reagents plus 5×10^{-6} M EDTA. All solutions were placed in an incubator at 22 °C and shaken in the dark for 2 hours before the DPASV measurement.

3.3.5.2.2 DPASV measurements of Cu-2,5-DMBQ complexes

The measurement procedure was generally similar to the experiments with 2,3-DHBA as described above with a few exceptions. A deposition time of 30 sec with an applied electrode potential of -200 mV was allowed to obtain sufficient sensitivity (S, $nA\bullet\mu M^{-1}$) with the ASV measurement, and an initial potential of -600mV and an ending potential of 400mV (vs. Ag/AgCl reference electrode) were used. The oxidation peak potential of Cu-2,5-DMBQ complexes was between –30mV and -200mV, which shifted depending on the pH. As before, the height of current peak was proportional to the concentration of labile Cu species, including the Cu-2,5-DMBQ complexes, and as such, the peak height decreased when EDTA was added.

3.3.6 Application of the theory of competitive ligand exchange and calculation of stability constants

3.3.6.1 Cu-2,3-DHBA-EDTA system

The calculation of stability constants of Cu-2,3-DHBA-EDTA system is described as below:

Free aquo Cu ion concentration [Cu^{2+}] can be calculated from equilibrium relationships with the 2,3 DHBA complexes. The total concentration of dissolved Cu in the water sample in absence of EDTA is given by:

$$[Cu]_T = [Cu^{2+}] + [Cu]_{in} + \sum [Cu(DHBA)_i] \quad (3\text{-}1)$$

where $[Cu]_{in}$ and $\Sigma[CuDHBA_i]$ represent Cu concentrations as inorganic complexes and complexes with 2,3-DHBA, respectively. The 2,3-DHBA complexes can then be determined by DPASV, together with $[Cu]_{in}$:

$$[Cu]_T = [Cu^{2+}] + [Cu]_{in} + \sum [Cu(DHBA_i)] = i_p / S \quad (3\text{-}2)$$

where i_p (ampere, A) is the peak current and S ($A \cdot M^{-1}$) is the electrode sensitivity.

If, in the presence of EDTA and 2,3-DHBA and EDTA, the dissolved copper after equilibration is distributed as follows:

$$[Cu]_T = [Cu^{2+}] + [Cu]_{in} + \sum [Cu(DHBA)_i] + \sum [Cu(EDTA)_i] \quad (3\text{-}3)$$

where, $\Sigma[Cu(EDTA_i)]$ is the concentration of Cu-EDTA complexes. Then, the 2,3-DHBA complexes can be determined selectively by DPASV, together with $[Cu]_{in}$:

$$[Cu^{2+}] + [Cu]_{in} + \sum [Cu(DHBA_i)] = i_e / S \quad (3\text{-}4)$$

Maintaining the same total Cu concentration in the absence and presence of EDTA, the difference between Equations 3-2 and 3-4 is the concentration of Cu-EDTA complexes:

$$\sum[Cu(EDTA_i)] = i_p / S - i_e / S = [Cu]_T - i_e / S \quad (3\text{-}5)$$

Equation 3-3 can be rewritten as:

$$[Cu]_T = [Cu^{2+}](1 + \alpha_{in} + \alpha_{DHBA}) + \sum[Cu(EDTA_i)] = i_e / S + \sum[Cu(EDTA_i)] \quad (3\text{-}6)$$

where α_{in} is the inorganic complexation coefficient, equal to the ratio of the concentrations of inorganic complexes to free cupric ions, as calculated from the major ion composition and pH of the sample. For the synthetic solution,

$$\alpha_{in} = \sum \beta_{iOH}[OH^-]^i \quad (3\text{-}7)$$

where β_i represents the stability constants of the *i*th Cu complex with a specified inorganic ligand *i* such as OH^-. α_{DHBA} is the 2,3-DHBA complexation coefficient, equal to the ratio of the concentrations of Cu-2,3-DHBA complexes to free cupric ions, and can be calculated as below:

$$\alpha_{DHBA} = \beta_{1DHBA}[H^+][DHBA^{3-}] + \beta_{2DHBA}[H^+]^2[DHBA^{3-}] + \beta_{3DHBA}[H^+]^2[DHBA^{3-}]^2 \quad (3\text{-}8)$$

where β_{1DHBA}, β_{2DHBA} and β_{3DHBA} represent the stability constants of $CuHDHBA^0$, CuH_2DHBA^+ and $Cu(HDHBA)_2^{2-}$ complexes, respectively.

The concentration of free deprotonated 2,3-DHBA, $[DHBA^{3-}]$, was calculated from mass balance and the acid dissociation equilibria of 2,3-DHBA:

$$[DHBA^{3-}] = \frac{[DHBA]_T}{1 + [H^+]/K_3 + [H^+]^2/K_2K_3 + [H^+]^3/K_1K_2K_3} \quad (3\text{-}9)$$

where K_1, K_2 and K_3 stand for the first, second and third protonation constant of 2,3-DHBA.

Therefore, $[Cu^{2+}]$ in the presence of EDTA can be calculated from Equation 3-6:

$$[Cu^{2+}](1+\alpha_{in}+\alpha_{DHBA}) = i_e/S \tag{3-10}$$

then,

$$[Cu^{2+}] = \frac{i_e/S}{1+\alpha_{in}+\alpha_{DHBA}} \tag{3-11}$$

The concentration of Cu-2,3-DHBA complexes were then calculated from Equation 3-12:

$$\sum[Cu(DHBA_i)] = [Cu^{2+}]\alpha_{DHBA} \tag{3-12}$$

The stability constants for the complexation of Cu with 2,3-DHBA and EDTA can be found in the literature. An equilibrium speciation computer program, MICROQL[62], was used to predicted Cu distribution among inorganic ligands, 2,3-DHBA and EDTA. The model results were compared to the experimental data calculated from above equations to verify the CLE/ASV method.

3.3.6.2 Cu-2,5-DMBQ-EDTA system

For Cu-2,5-DMBQ-EDTA system, the total concentration of dissolved Cu in the water sample in the presence of EDTA is given by:

$$[Cu]_T = [Cu^{2+}] + [Cu]_{in} + \sum[Cu(DMBQ)_i] + \sum[Cu(EDTA)_i] = i_e/S + \sum[Cu(EDTA)_i] \tag{3-13}$$

where $\Sigma[Cu(DMBQ)_I]$ represents the Cu-2,5-DMBQ complexes.

The concentration of Cu-EDTA complexes were obtained from equation 3-13 with the known total concentration of Cu and the electrode sensitivity, *S*, as described above. By varying the total concentration of Cu, data for Cu-EDTA concentrations as a function

of total Cu, EDTA and 2,5-DMBQ concentrations were obtained at different pHs. These data were fitted to a set of equilibrium reactions describing the speciation of Cu in the presence of EDTA and 2,5-DMBQ using a computer program, FITEQL[63]. The program output is the fitted values for the Cu-2,5-DMBQ stability constants.

3.4 Cyclic voltammetry method

The instrument used for cyclic voltammetry was the same as described in section 3.3.4, with the exception that the working electrode was a glassy carbon electrode with a surface area of 0.126cm^2. The cyclic voltammetry measurements were conducted at room temperature. Ultrapure argon was passed through the solution for 15min before taking the measurements. The glassy carbon electrode was polished for 10 seconds with small, circular movements with 0.5μm alumina (Al_2O_3) compound on a polishing pad, rinsed with D.I. water, immersed in diluted HCl for 10s, rinsed again with D.I. water and dried with a cloth or filter paper before use. The glassy carbon electrode was introduced into the voltametric cell immediately before scanning. The cyclic voltammetry scan rates were 2000 mV/s and 500mV/s. The resulting scan curves were recorded by the 746 VA trace analyzer, and the data from the resulting scans were saved in a personal computer.

CHAPTER 4

RESULTS AND DISCUSSION

4.1 Competitive ligand exchange/Anodic stripping voltammetry (CLE/ASV) study

4.1.1 CLE/ASV study with 2,3-DHBA

4.1.1.1 Anodic stripping voltammetry of Cu-2,3-DHBA-EDTA system

Differential Pulse Anodic Stripping Voltammetry (DPASV) measurements were conducted on the solutions with Cu and 2,3-DHBA, and with Cu, 2,3-DHBA and EDTA by varying total Cu concentration at different pHs. Preliminary experimental results indicated that the Cu-2,3-DHBA complexes were fully labile ligands that produce a current peak at a specific potential. In solutions that contained excess 2,3-DHBA, this current peak was proportional to the Cu concentration. A typical voltammogram of a Cu-2,3-DHBA complex is shown in Figure 4.1.

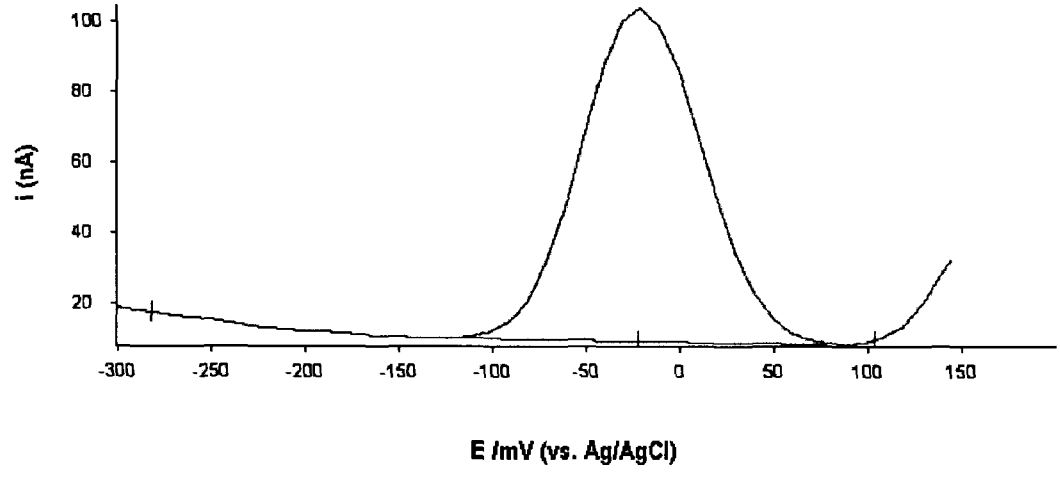

Figure 4.1: Anodic stripping voltammogram for Cu-2,3-DHBA complexes (5×10^{-7}M Cu, 5×10^{-5}M 2,3-DHBA, pH=5.0 (0.03M acetate buffer) and 0.01M KNO_3).

The specific peak potential for Cu-2,3-DHBA complexes at the conditions shown in Figure 4.1 is -23mV, which increases with Cu concentration and decreases with pH as shown in Figure 4.2. The height of the current peak corresponds to the labile species of Cu, which include free Cu ions, the complexes of Cu and inorganic ligands such as OH^- in this case, and Cu-2,3-DHBA complexes. In presence of the competitive ligand EDTA, the height of the current peak decreases because the Cu-EDTA complexes are inert species that do not react on the surface of electrode.

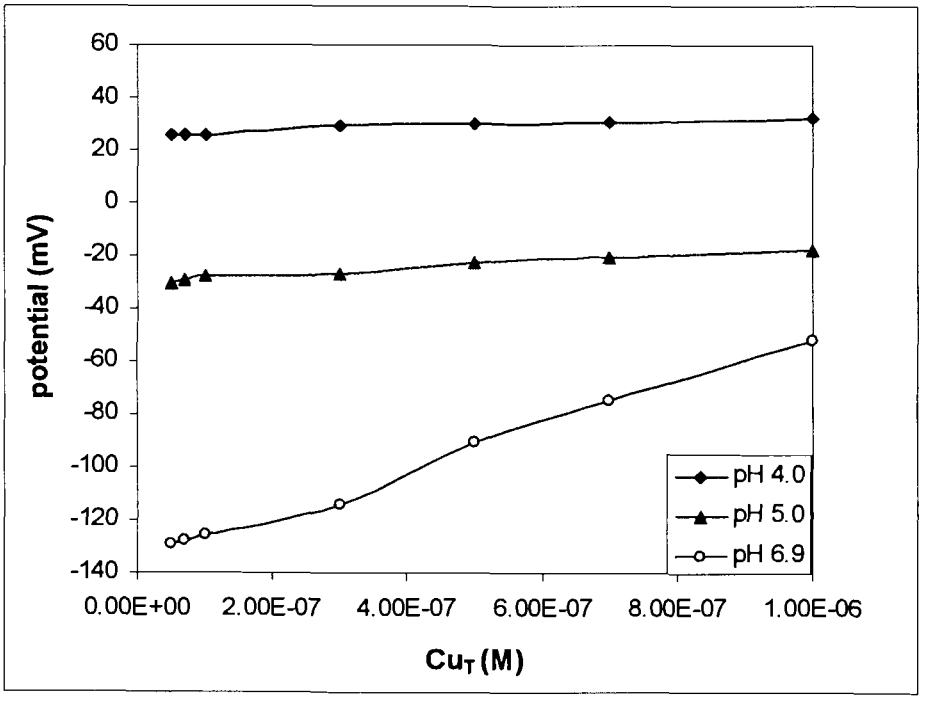

Figure 4.2: Peak potential for Cu-DHBA complexes vs. Cu concentration at different pHs (5×10^{-8}~1×10^{-6}M Cu, 5×10^{-5}M 2,3-DHBA, 0.03M acetate buffer and 0.01M KNO_3).

Figures 4.3 though 4.8 illustrate the DPASV experimental results at different concentrations of Cu, 2,3-DHBA and EDTA, and at different pH values.

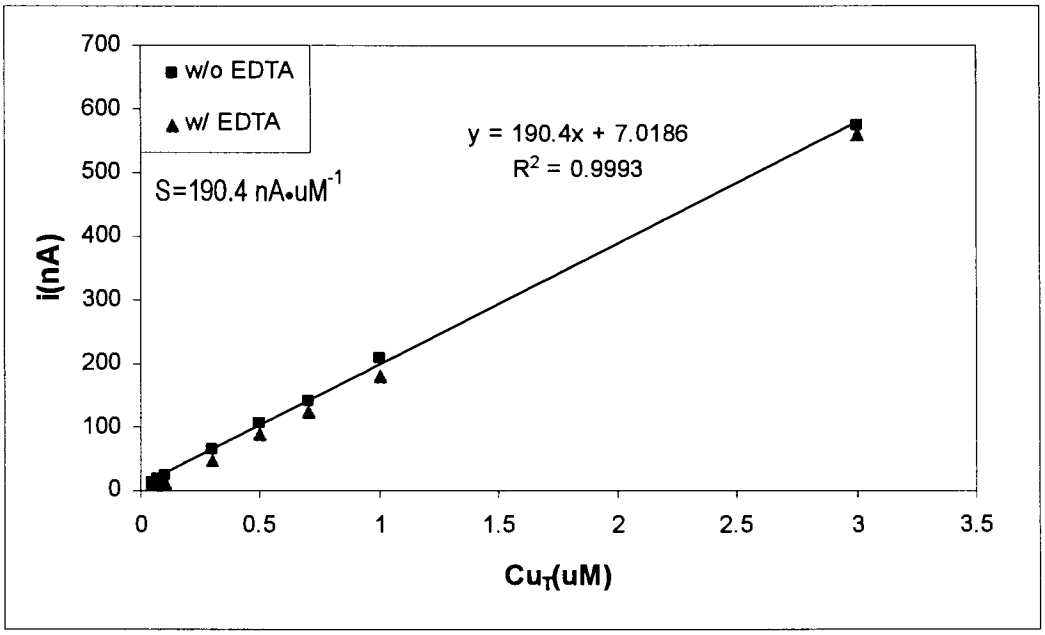

Figure 4.3: DPASV experimental results: current peaks of Cu-2,3-DHBA complexes at pH 4 (5×10^{-8}~3×10^{-6}M Cu, 5×10^{-5}M 2,3-DHBA, 1×10^{-7}M EDTA, 0.03M acetate buffer and 0.01M KNO_3, deposit time=60s).

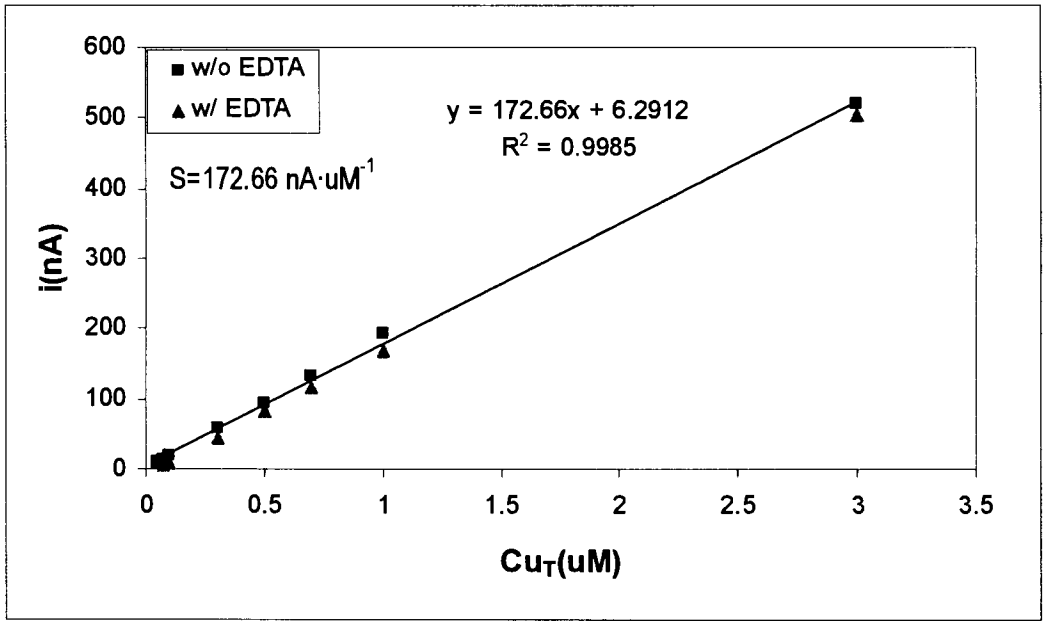

Figure 4.4: DPASV experimental results: current peaks of Cu-2,3-DHBA complexes at pH 5 (5×10^{-8}~3×10^{-6}M Cu, 5×10^{-5}M 2,3-DHBA, 1×10^{-7}M EDTA, 0.03M acetate buffer and 0.01M KNO_3, deposit time=60s).

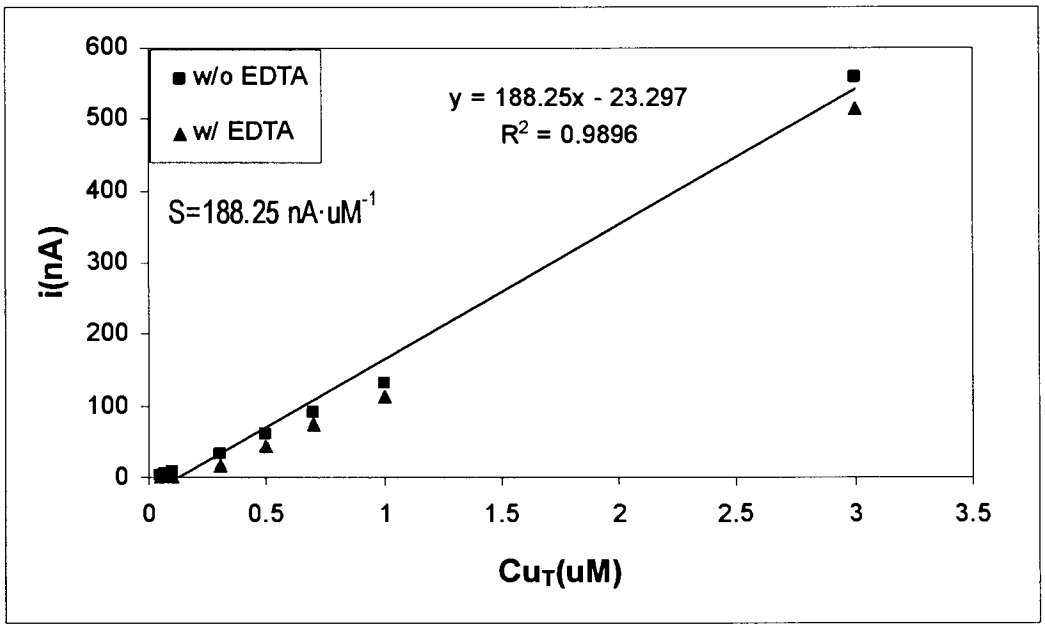

Figure 4.5: DPASV experimental results: current peaks of Cu-2,3-DHBA complexes at pH 6.9 (5×10^{-8}~3×10^{-6}M Cu, 5×10^{-5}M 2,3-DHBA, 1×10^{-7}M EDTA, 0.03M HEPES buffer and 0.01M KNO_3, deposit time=60s).

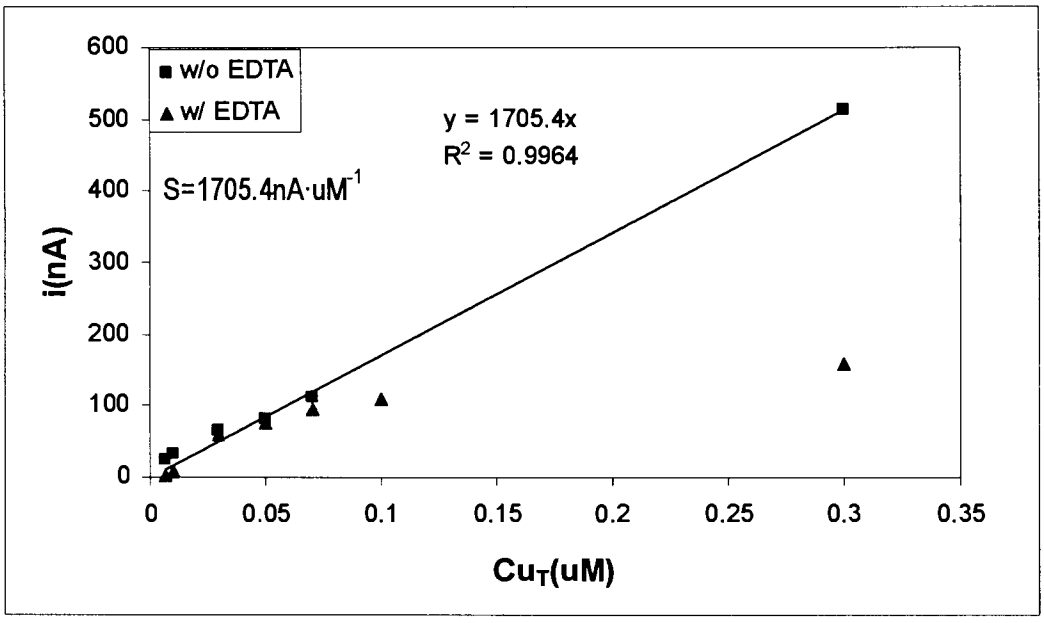

Figure 4.6: DPASV experimental results: current peaks of Cu-2,3-DHBA complexes at pH 4 (7×10^{-9}~3×10^{-7}M Cu, 5×10^{-5}M 2,3-DHBA, 5×10^{-9}M EDTA, 0.03M acetate buffer and 0.01M KNO_3, deposit time=180s).

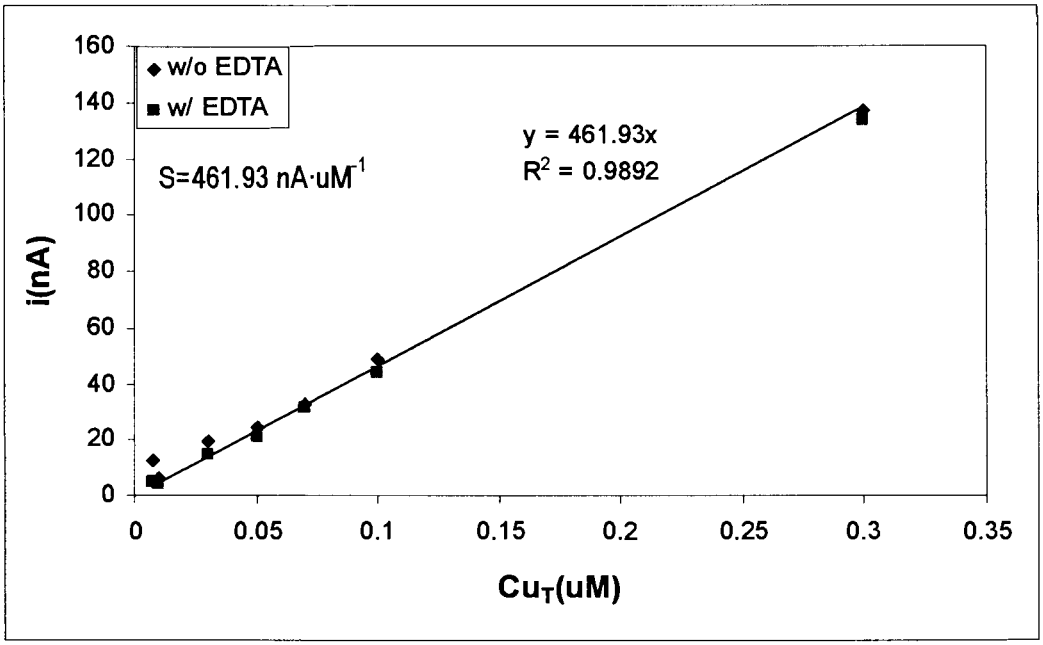

Figure 4.7: DPASV experimental results: current peaks of Cu-2,3-DHBA complexes at pH 5 (7×10^{-9}~3×10^{-7}M Cu, 5×10^{-5}M 2,3-DHBA, 5×10^{-9}M EDTA, 0.03M acetate buffer and 0.01M KNO_3, deposit time=180s).

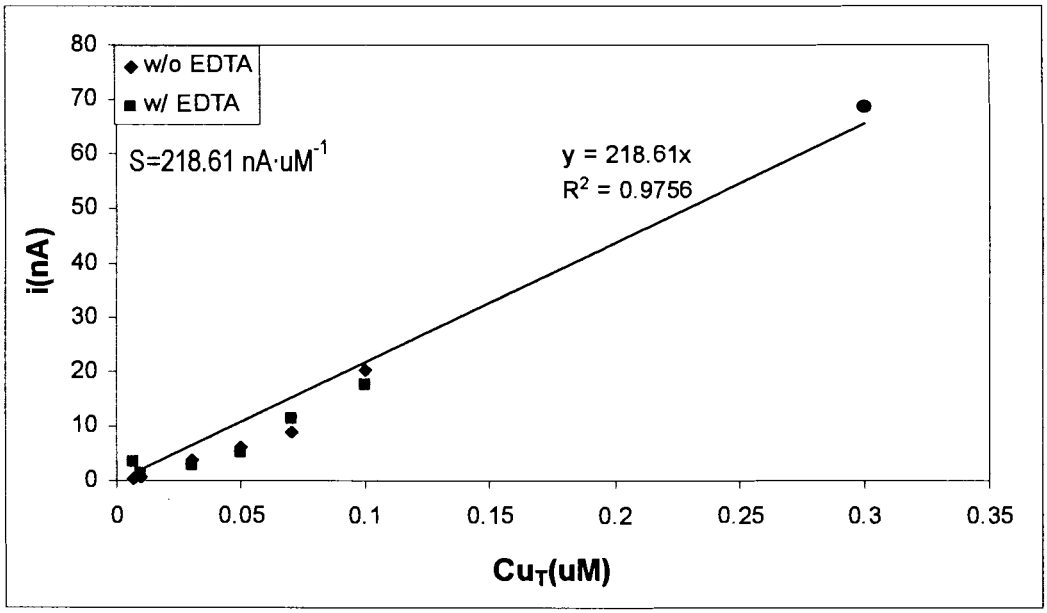

Figure 4.8: DPASV experimental results: current peaks of Cu-2,3-DHBA complexes at pH 6.9 (7×10^{-9}~3×10^{-7}M Cu, 5×10^{-5}M 2,3-DHBA, 5×10^{-9}M EDTA, 0.03M HEPES buffer and 0.01M KNO_3, deposit time=180s).

In Figures 4.3 through 4.8, the slope of the trend lines (S) of the experimental data without EDTA represents the sensitivity of the electrode, which has a unit of $nA \cdot \mu M^{-1}$. In Figures 4.3 through 4.5, 1×10^{-7}M EDTA was used to compete with 5×10^{-5}M 2,3-DHBA for Cu concentrations ranging from 5×10^{-8}M to 3×10^{-6}M. In Figure 4.6 through 4.8, 5×10^{-9}M EDTA was used to compete with 5×10^{-5}M 2,3-DHBA for Cu concentrations ranging from 7×10^{-9}M to 3×10^{-7}M. In both above conditions, the peak currents (i_p) are lower in the presence of EDTA compared with that without EDTA (i_e). From the difference between i_p and i_e, the free aquo Cu ion concentration $[Cu^{2+}]$, the concentration of Cu-2,3-DHBA complexes, $\Sigma[Cu(DHBA)_i]$, and the concentration of Cu-EDTA complexes, $\Sigma[Cu(EDTA)_i]$, can be calculated using the equations described in section 3.3.6.1. This was done using the known stability constants for Cu inorganic species and 2,3-DHBA species.

4.1.1.2 Calculation of Cu-2,3-DHBA complexes from the experimental data

The concentration of Cu-2,3-DHBA complexes were obtained by multiplying the concentration of free aquo Cu ions $[Cu^{2+}]$ and the 2,3-DHBA complexation coefficient α_{DHBA} (Equation 3-12). The 2,3-DHBA complexation coefficient, α_{DHBA}, was calculated from equation 3-8:

$$\alpha_{DHBA} = \beta_{1DHBA}[H^+][DHBA^{3-}] + \beta_{2DHBA}[H^+]^2[DHBA^{3-}] + \beta_{3DHBA}[H^+]^2[DHBA^{3-}]^2 \quad (3\text{-}8)$$

The relevant stability constants are reported in Table 4.1.

The concentration of free deprotonated 2,3-DHBA, $[DHBA^{3-}]$, was calculated from the mass balance values and the acid dissociation equilibria of 2,3-DHBA as described in equation 3-9:

Table 4.1: Dissociation reactions and related stability constants for Cu-2,3-DHBA-EDTA systems (constants are used to calculate speciation distribution).

Dissociation reaction	Symbol	logK
$CuHDHBA^{0} \leftrightarrow Cu^{2+} + H^{+} + DHBA^{3-}$	β_{1DHBA}	20.7[64]
$CuH_2DHBA^{+} \leftrightarrow Cu^{2+} + 2H^{+} + DHBA^{3-}$	β_{2DHBA}	25.04[64]
$Cu(HDHBA)_2^{2-} \leftrightarrow Cu^{2+} + 2H^{+} + 2DHBA^{3-}$	β_{3DHBA}	40.26[64]
$H_3DHBA^{0} \leftrightarrow H_2DHBA^{-} + H^{+}$	K_1	2.68[64]
$H_2DHBA^{-} \leftrightarrow HDHBA^{2-} + H^{+}$	K_2	9.84[64]
$HDHBA^{2-} \leftrightarrow DHBA^{3-} + H^{+}$	K_3	13.1[64]
$CuOH^{+} \leftrightarrow Cu^{2+} + OH^{-}$	β_{1OH}	6.3[65]
$Cu(OH)_2^{0} \leftrightarrow Cu^{2+} + 2OH^{-}$	β_{2OH}	11.8[65]
$Cu(OH)_4^{2-} \leftrightarrow Cu^{2+} + 4OH^{-}$	β_{4OH}	16.4[65]
$H_5EDTA^{+} \leftrightarrow H_4EDTA^{0} + H^{+}$	K_{1EDTA}	1.0[65]
$H_4EDTA^{0} \leftrightarrow H_3EDTA^{-} + H^{+}$	K_{2EDTA}	2.72[65]
$H_3EDTA^{-} \leftrightarrow H_2EDTA^{2-} + H^{+}$	K_{3EDTA}	3.24[65]
$H_2EDTA^{2-} \leftrightarrow HEDTA^{3-} + H^{+}$	K_{4EDTA}	6.68[65]
$HEDTA^{3-} \leftrightarrow EDTA^{4-} + H^{+}$	K_{5EDTA}	11.12[65]
$CuEDTA^{2-} \leftrightarrow Cu^{2+} + EDTA^{4-}$	β_{1EDTA}	20.5[65]
$CuHEDTA^{-} \leftrightarrow Cu^{2+} + EDTA^{4-} + H^{+}$	β_{2EDTA}	23.9[65]
$CuOHEDTA^{3-} \leftrightarrow Cu^{2+} + EDTA^{4-} + OH^{-}$	β_{3EDTA}	22.6[65]

$$[DHBA^{3-}] = \frac{[DHBA]_T}{1+[H^+]/K_3 + [H^+]^2/K_2K_3 + [H^+]^3/K_1K_2K_3} \quad (3\text{-}9)$$

The protonation constants of 2,3-DHBA, K_1, K_2 and K_3 are reported in Table 4.1. The concentration of free aquo Cu ions, $[Cu^{2+}]$, was calculated from equation 3-11:

$$[Cu^{2+}] = \frac{i_e/S}{1+\alpha_{in}+\alpha_{DHBA}} \quad (3\text{-}11)$$

where i_e is the peak current in presence of EDTA, S is the electrode sensitivity, and the inorganic complexation coefficient α_{in} can be calculated from equation 3-7:

$$\alpha_{in} = \sum \beta_{iOH}[OH^-]^i \quad (3\text{-}7)$$

The stability constants of the *i*th Cu complex with a specified inorganic ligand *i* such as OH^- are reported in Table 4.1. The stability constants of EDTA and Cu-EDTA complexes are also reported in Table 4.1.

With these known stability constants, Cu species distribution among inorganic species OH^-, 2,3-DHBA and EDTA at different pHs were predicted using the computer program, MICROQL[62]. A comparison between the model predicted data and the experimental data then allowed an assessment of the feasibility for application of the competitive ligand exchange method in the acidic aqueous conditions used in this study as outlined below.

4.1.1.3 Comparison of experimental data and model predicted data

Figures 4.9 through 4.14 show the comparison between the experimental data of Cu species distribution of Cu-2,3-DHBA-EDTA system, and the model predicted results at different pHs and different total Cu concentrations. Logarithmic (log-log) plots of free

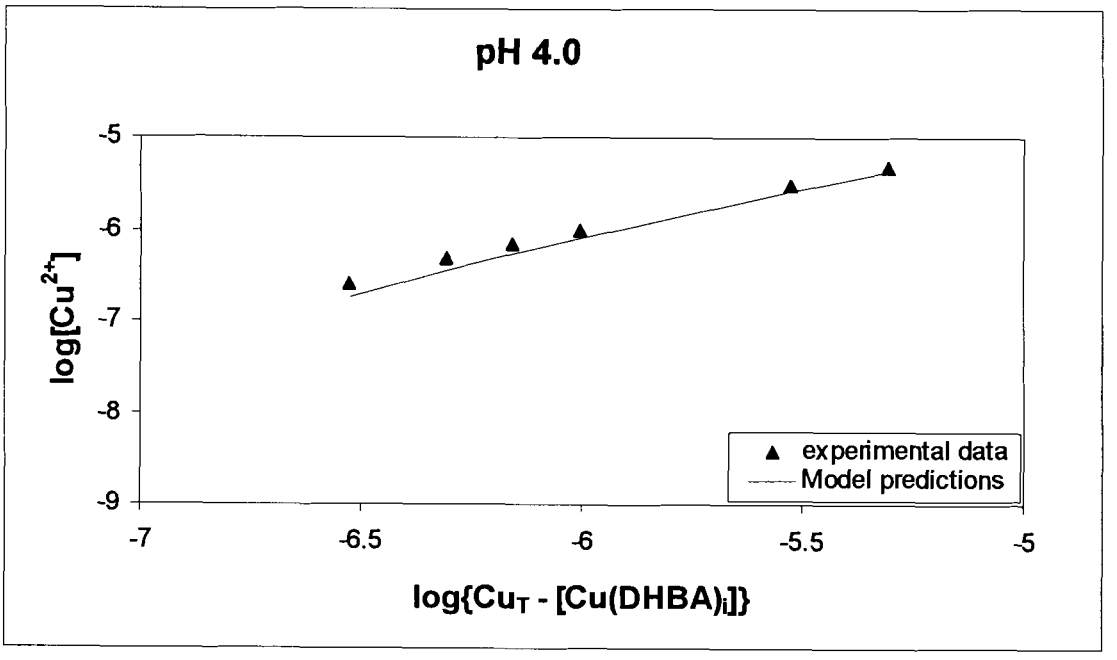

Figure 4.9: Comparison of experimental data and model predicted data at pH 4 with 3×10^{-7}~5×10^{-6}M Cu, 5×10^{-5}M 2,3-DHBA, 1×10^{-7}M EDTA.

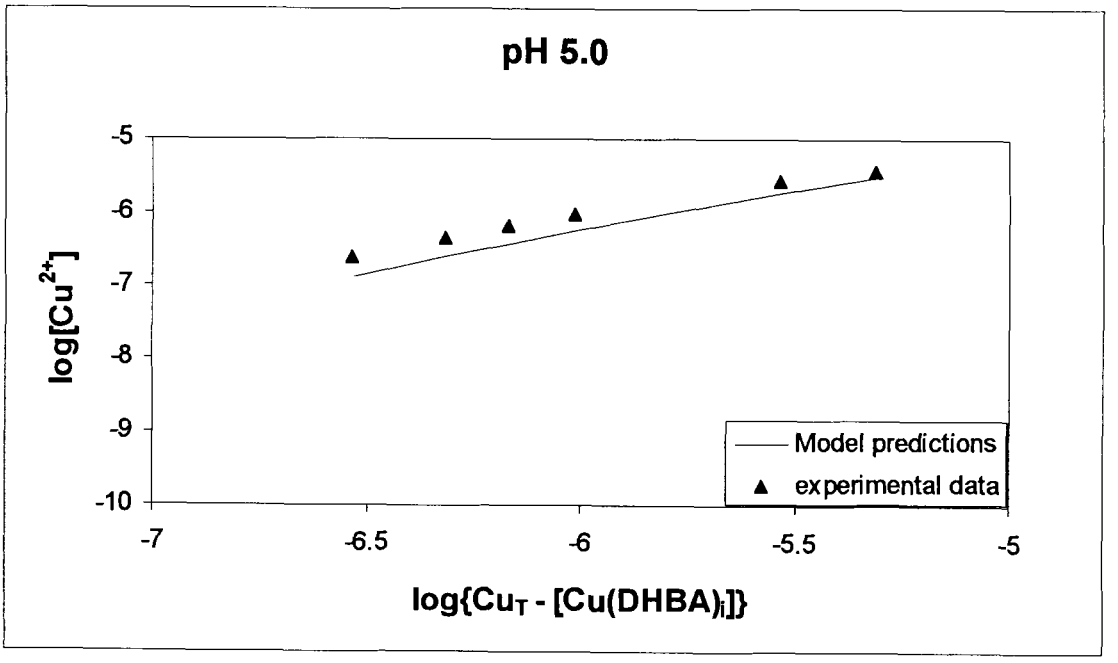

Figure 4.10: Comparison of experimental data and model predicted data at pH 5 with 3×10^{-7}~5×10^{-6}M Cu, 5×10^{-5}M 2,3-DHBA, 1×10^{-7}M EDTA.

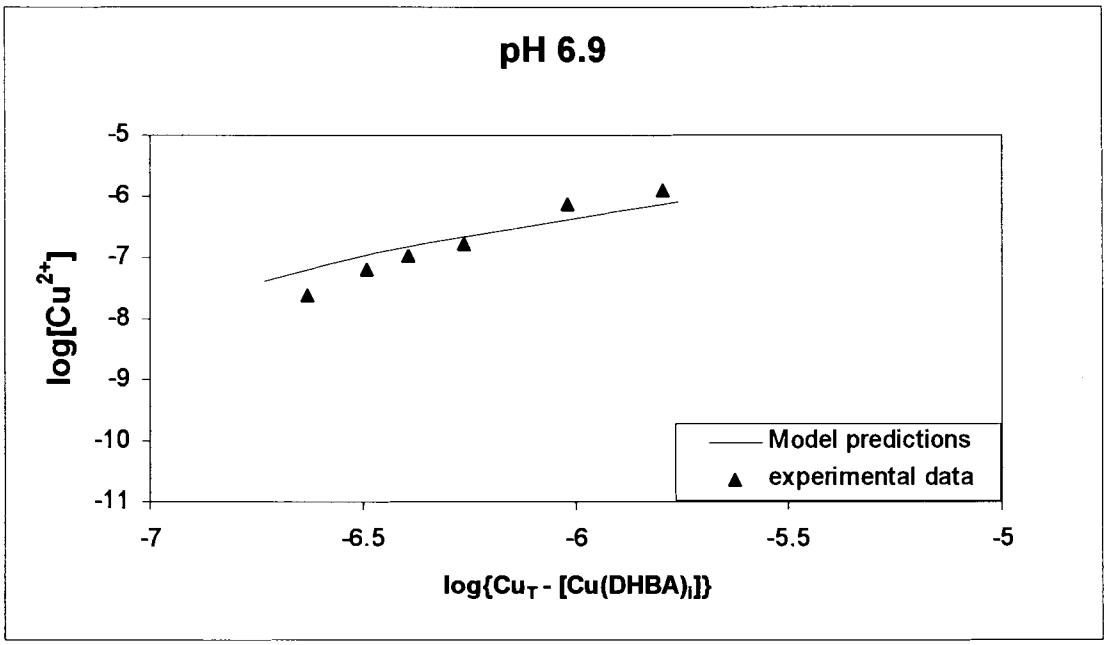

Figure 4.11: Comparison of experimental data and model predicted data at pH 6.9 with 3×10^{-7}~5×10^{-6}M Cu, 5×10^{-5}M 2,3-DHBA, 1×10^{-7}M EDTA.

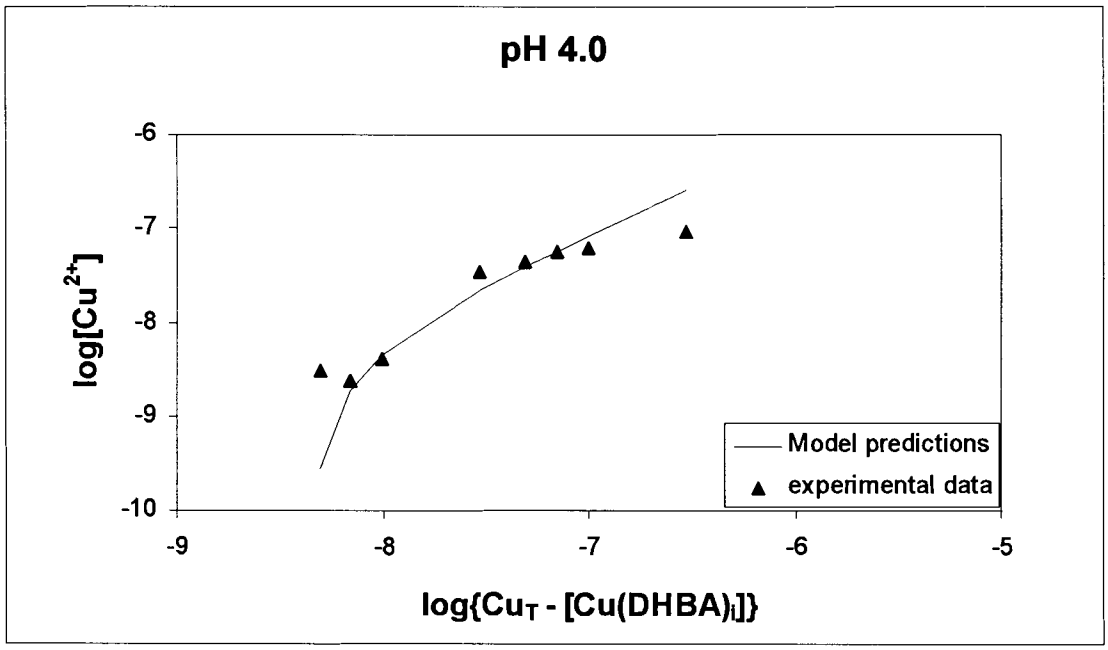

Figure 4.12: Comparison of experimental data and model predicted data at pH 4 with 5×10^{-9}~3×10^{-7}M Cu, 5×10^{-5}M 2,3-DHBA, 5×10^{-9}M EDTA.

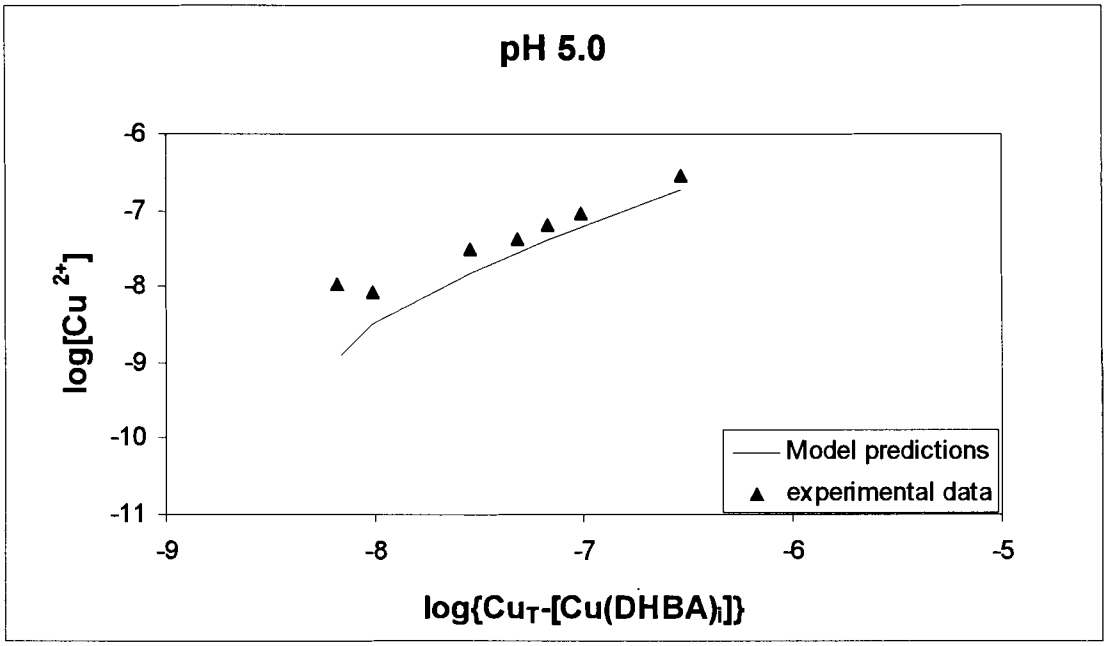

Figure 4.13: Comparison of experimental data and model predicted data at pH 5 with 5×10^{-9}~3×10^{-7}M Cu, 5×10^{-5}M 2,3-DHBA, 5×10^{-9}M EDTA.

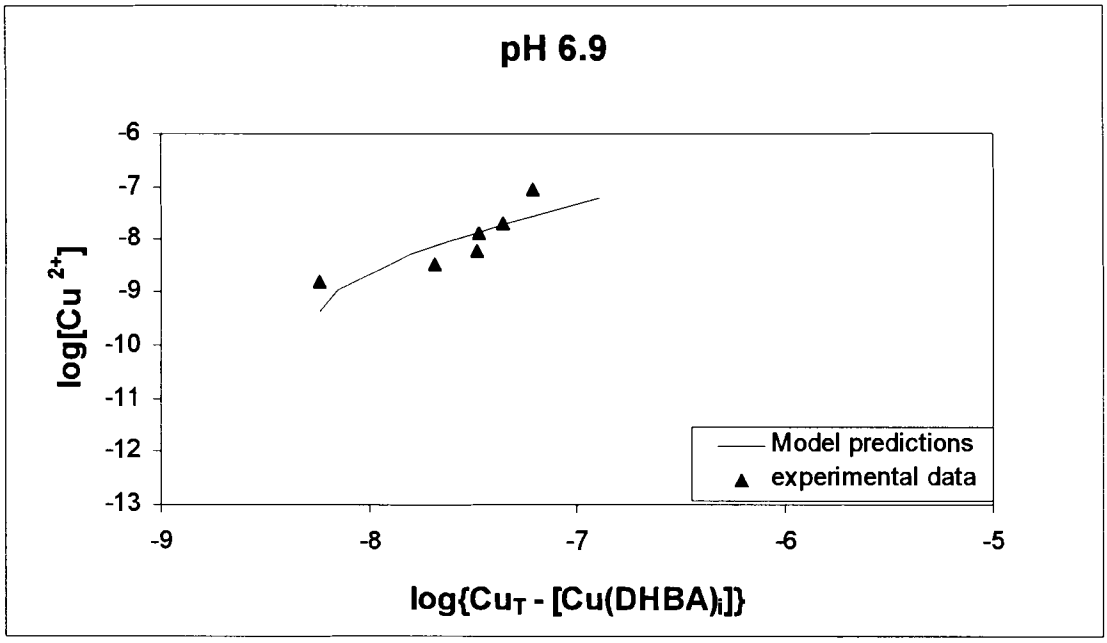

Figure 4.14: Comparison of experimental data and model predicted data at pH 6.9 with 5×10^{-9}~3×10^{-7}M Cu, 5×10^{-5}M 2,3-DHBA, 5×10^{-9}M EDTA.

aquo Cu concentration, $[Cu^{2+}]$, vs. total Cu minus the concentration of Cu-2,3-DHBA complexes, $\{Cu_T-[Cu(DHBA)_i]\}$, were used here as adapted from Xue, H. and Sigg, L[66].

Figures 4.9 through 4.14 show that the model predictions (free aquo Cu ion concentrations calculated using the computer program MICROQL) match the experimental data well at all pH values studied here. This correspondence between the experimental and model predicted data suggests that it is feasible to use the CLE/DPASV method to study chemical speciation for the Cu-DHBA-EDTA system. If the stability constants for Cu and 2,3-DHBA complexes are unknown, chemical speciation modeling of the complexation data obtained from the CLE/DPASV experiments for the Cu-2,3-DHBA-EDTA system can be used to determine such stability constants.

4.1.2 Competitive ligand exchange study for the Cu, 2,5-dimethoxybenzoquinone system

4.1.2.1 Anodic stripping voltammetry of Cu-2,5-DMBQ-EDTA system

Differential Pulse Anodic Stripping Voltammetry measurements were conducted on solutions containing Cu and 2,5-DMBQ, and Cu, 2,5-DMBQ and EDTA by varying the total Cu concentrations at different pHs. Cu-2,5-DMBQ complexes are fully labile ligands which give a current peak at a specific potential. In the presence of excess 2,5-DMBQ in solution, this current peak is proportional to the Cu bound by the ligand. A typical voltammogram for Cu-2,5-DMBQ complexes is shown in Figure 4.15.

The peak potential for Cu-2,5-DMBQ complexes at the conditions shown in Figure 4.15 is at -136mV, which decreases with Cu concentration and with pH as shown in Figure 4.16. The height of the current peak corresponds to the concentration of labile species of Cu, which include free Cu ions, the complexes of Cu and inorganic ligands such as OH^-, and Cu-2,5-DMBQ complexes. In presence of the competitive ligand EDTA,

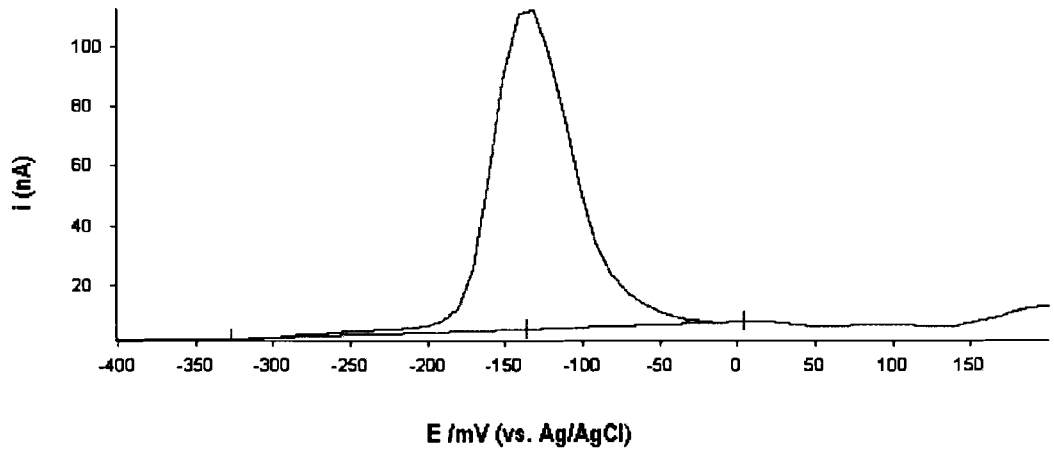

Figure 4.15: Anodic stripping voltammogram for Cu-2,5-DMBQ complexes (5×10^{-7}M Cu, 3×10^{-5}M 2,5-DMBQ, pH=5.0(0.03M acetate buffer) and 0.12M KNO_3).

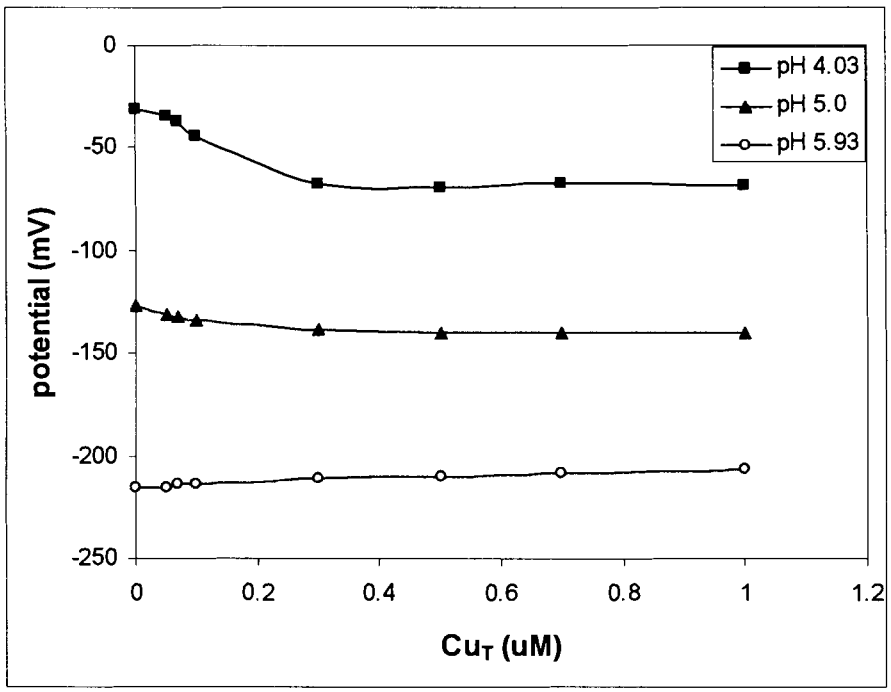

Figure 4.16: Peak potential for Cu-DMBQ complexes vs. Cu concentration at different pHs ($0\sim1\times10^{-6}$M Cu, 2.5×10^{-5}M 2,5-DMBQ at pH 4.03 and 3×10^{-5}M 2,5-DMBQ at pH 5.0 and 5.93 in order to get good sensitivity of the ASV measurement, 0.03M acetate buffer and 0.01M KNO_3).

the height of the current peak decreases because the Cu-EDTA complexes are inert species that do not react at the surface of electrode, and therefore, cannot generate a current peak during voltammetric measurements.

Figures 4.17 though 4.19 illustrate the DPASV experimental results at different concentrations of Cu, 2,5-DMBQ and EDTA, and at different pH values.

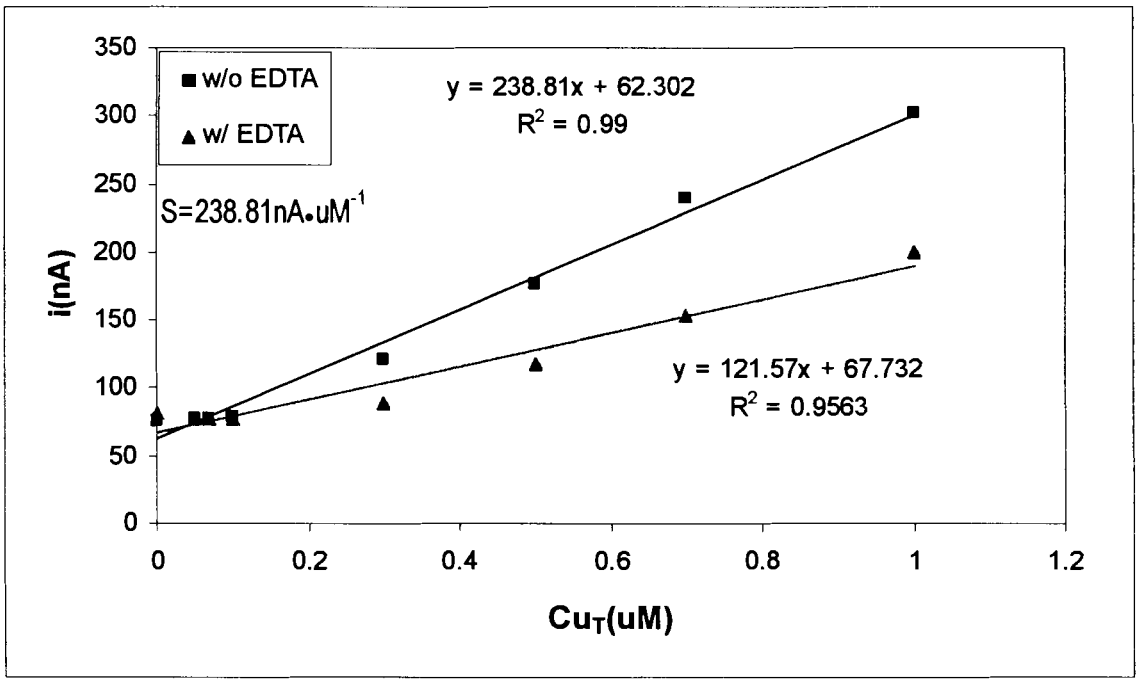

Figure 4.17: DPASV experimental results: current peaks of Cu-2,5-DMBQ complexes at pH 4.03 (5×10^{-8}~1×10^{-6}M Cu, 2.5×10^{-5}M 2,5-DMBQ, 5×10^{-6}M EDTA, 0.03M acetate buffer and 0.12M KNO_3, deposit time=30s).

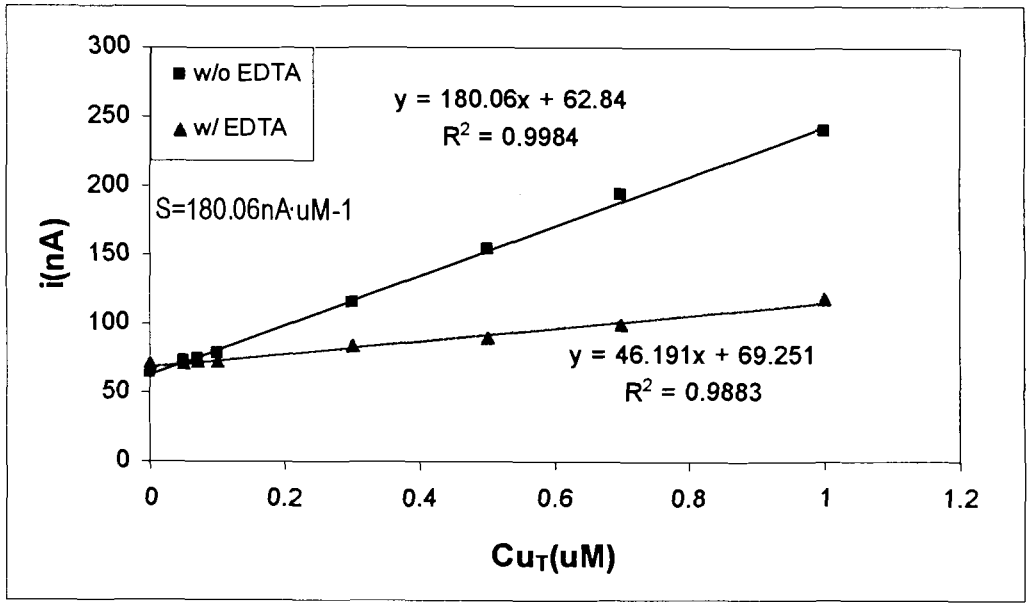

Figure 4.18: DPASV experimental results: current peaks of Cu-2,5-DMBQ complexes at pH 5.0 (5×10^{-8}~1×10^{-6}M Cu, 3.0×10^{-5}M 2,5-DMBQ, 5×10^{-6}M EDTA, 0.03M acetate buffer and 0.12M KNO_3, deposit time=30s).

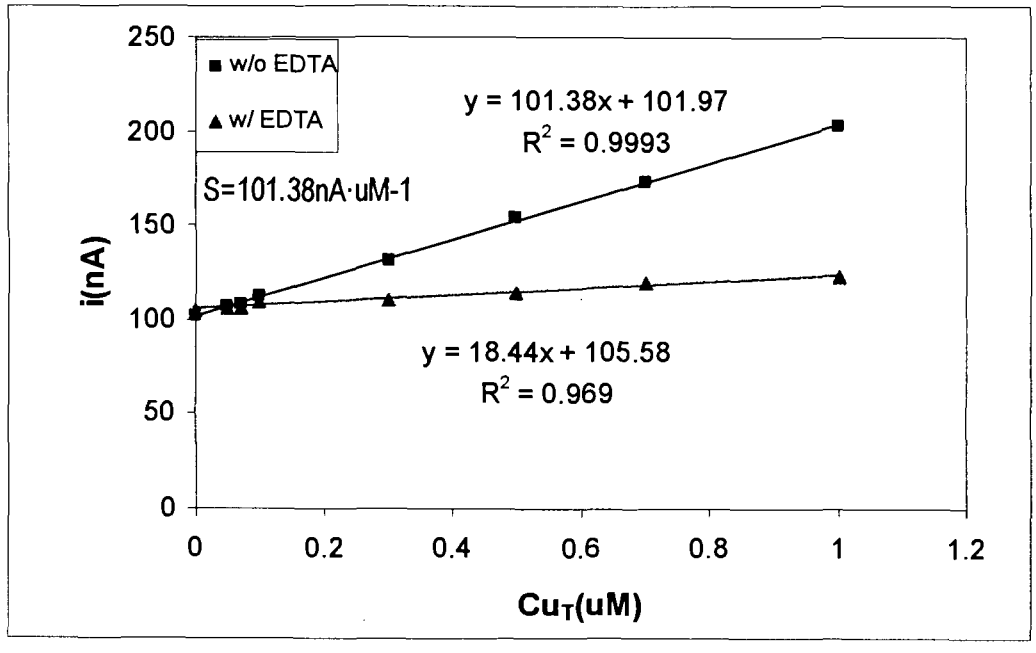

Figure 4.19: DPASV experimental results: current peaks of Cu-2,5-DMBQ complexes at pH 5.93 (5×10^{-8}~1×10^{-6}M Cu, 3.0×10^{-5}M 2,5-DMBQ, 5×10^{-6}M EDTA, 0.03M acetate buffer and 0.12M KNO_3, deposit time=30s).

In Figures 4.17 through 4.19, the slope (S) of the trend lines of the experimental data without EDTA represents the sensitivity of electrode. For these experiments, a Cu concentration range of 5×10^{-8}M to 1×10^{-6}M, an EDTA concentration of 5×10^{-6}M, and a 2,5-DMBQ concentration of 2.5×10^{-5}M at pH 4.03 were used. For pHs of 5.0 and 5.93, however, an EDTA concentration of 5×10^{-6}M, and a 2,5-DMBQ concentration of 3×10^{-5}M were used in order to get sufficient sensitivity (S, $nA\bullet\mu M^{-1}$) of the DPASV measurements. Under all experimental conditions, the peak current (i_p) is lower in presence of EDTA compared with that without EDTA (i_e) as anticipated because EDTA would irreversibly complex with copper reducing the current. From the difference between i_p and i_e, the concentration of Cu-EDTA complexes $\Sigma[Cu(EDTA)_i]$ can be calculated using equation 4.1.

$$\sum[Cu(EDTA)_i] = Cu_T - i_e/S \qquad (4\text{-}1)$$

The calculation results at three different pHs are shown in Table 4.2. These results were then used in the computer model FITEQL[63] to estimate the stability constants of Cu and 2,5-DMBQ complex.

Table 4.2: The concentration of Cu-EDTA complexes calculated from experimental data.

Cu_T (M)	$\Sigma[Cu(EDTA)_i]$ (M)		
	pH=4.03	pH=5.0	pH=5.93
5.00E-8	0.000E+00	4.350E-09	8.572E-09
7.00E-8	6.820E-09	1.769E-08	2.887E-08
1.00E-7	3.858E-08	4.191E-08	2.750E-08
3.00E-7	1.859E-07	1.842E-07	2.219E-07
5.00E-7	2.658E-07	3.496E-07	3.721E-07
7.00E-7	3.226E-07	4.955E-07	5.200E-07
1.00E-6	4.270E-07	6.941E-07	7.928E-07

4.1.2.2 The binding of Cu and 2,5-DMBQ

The structure of 2,5-DMBQ is illustrated in Figure 4.20(a). In the presence of excess2,5-DMBQ in solution, it is possible to have a 1 to 1 Cu-DMBQ complex; i.e., $CuDMBQ^{2+}$. Under acidic conditions, 2,5-DMBQ also can bind with protons to form $HDMBQ^{+}$ species. The structures of these two species are shown in Figure 4.20(b) and (c), respectively.

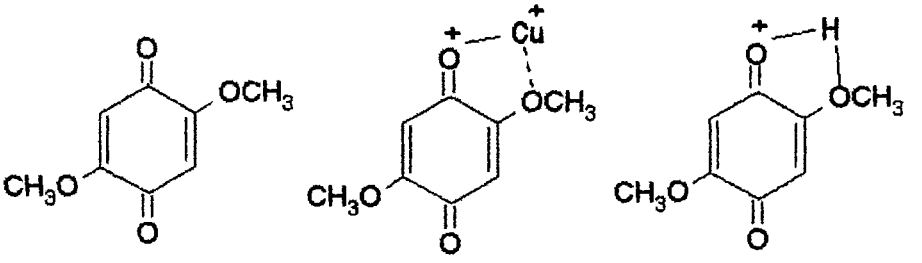

(a) 2,5-DMBQ (b) $CuDMBQ^{2+}$ (c) $HDMBQ^{+}$

Figure 4.20: The molecular structure of 2,5-DMBQ and its proposed Cu- and proton-bound species formed under experimental conditions.

4.1.2.3 Modeling of Cu-DMBQ binding

Two chemical species ($HDMBQ^{+}$ and $CuDMBQ^{2+}$) were used to model the experimental data shown in Table 4.2 to estimate the stability constants of these two species using the computer program FITEQL[63]. The best fitted values for the two species are shown in Table 4.3.

Table 4.3: Stability constants for the formation of $HDMBQ^{+}$ and $CuDMBQ^{2+}$ species.

Species	Dissociation reaction	log K
$HDMBQ^{+}$	$HDMBQ^{+} \leftrightarrow DMBQ + H^{+}$	15.94
$CuDMBQ^{2+}$	$CuDMBQ^{2+} \leftrightarrow DMBQ + Cu^{2+}$	22.52

Figure 4.21 shows the fitted results using the data in Table 4.2, and the resulting constants are reported in Table 4.3. Sensitivity analysis suggests that model simulation is indeed sensitive with respect to the fitted $HDMBQ^{+}$ and $CuDMBQ^{2+}$ complexation constants (Table 4.3). Figures 4.22a and 4.22b show that the sum of the squares of the difference between the experimental data and model simulations is at a minimum for the stability constants reported in Table 4.3.

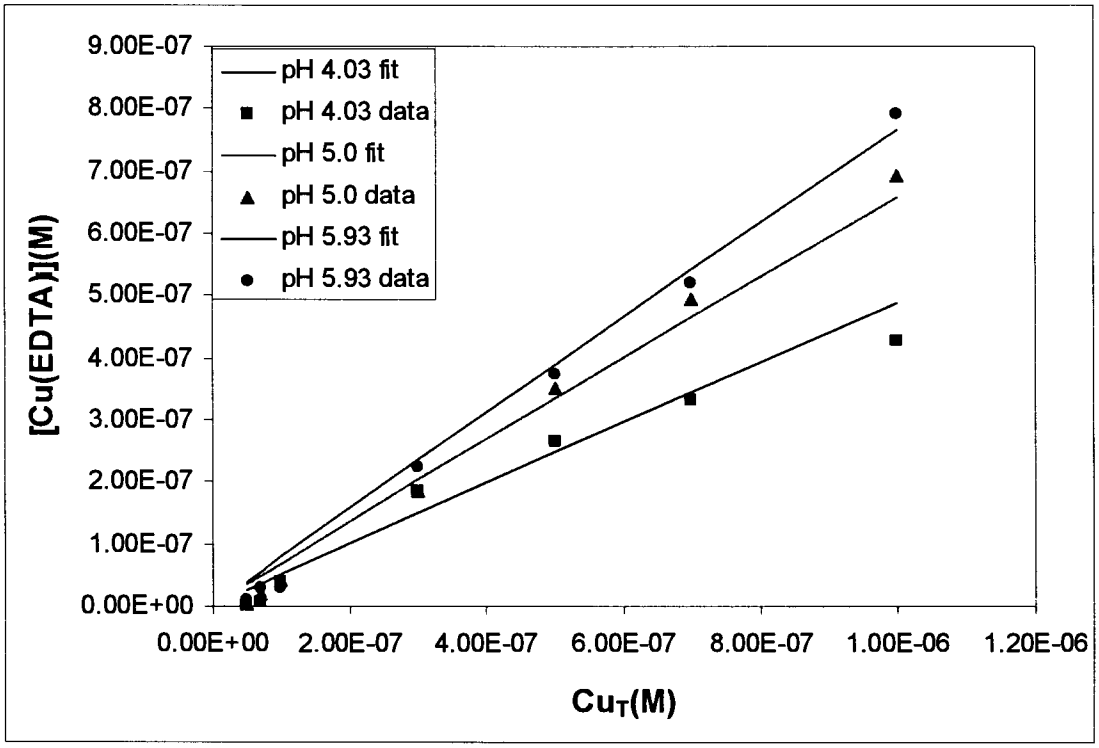

Figure 4.21: The fitted results given by FITEQL: for $HDMBQ^{+}$, log K=15.94 and for $CuDMBQ^{2+}$, log K=22.52

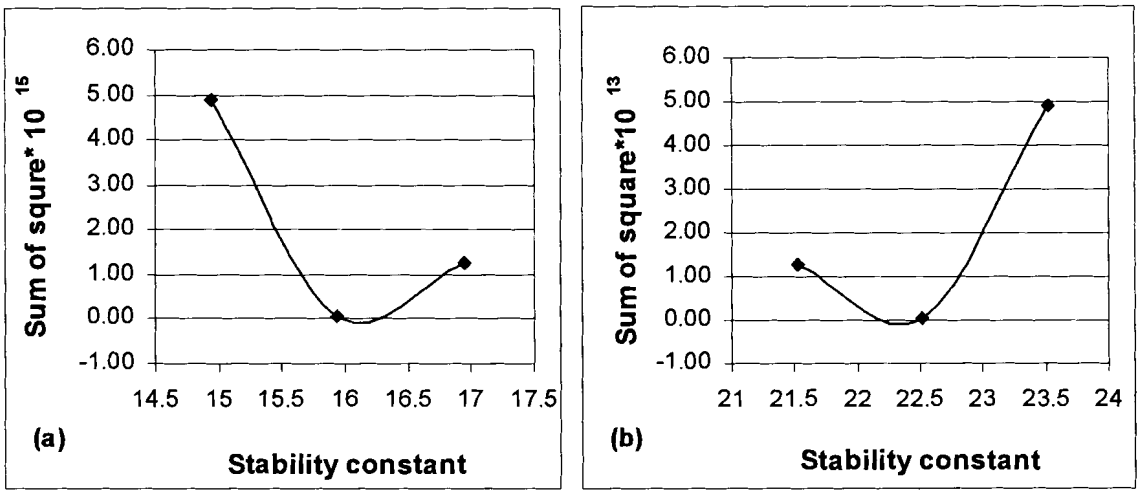

Figure 4.22: The fitting sensitivity of FITEQL. (a) Stability constant of $HDMBQ^{+}$; (b) stability constant of $CuDMBQ^{2+}$.

Figures 4.23 and 4.24 show, in the presence of EDTA, the species distribution of Cu and DMBQ at different pHs respectively. The speciation is calculated by MICROQL using the stability constants shown in Table 4.3. As shown in Figure 4.23, as the pH increases, the concentration of the Cu-DMBQ complex decreases and the concentration of the Cu-EDTA complex increases. Most of the DMBQ, however, remains in the protonated form according to the model for the stability constants developed here (Figure 4.24).

Figure 4.23 shows that at low pHs (2.5 and 4.03) 2,5-DMBQ has relatively strong binding affinity with Cu(II) compared with a strong metal chelator, EDTA. This may increase the solubility and availability of Cu(II) in the wood decay environment.

It has been proposed that oxalic acid produced by wood degrading fungi functions not only as a chelation agent to sequester iron from iron (hydr)oxide complexes, but also

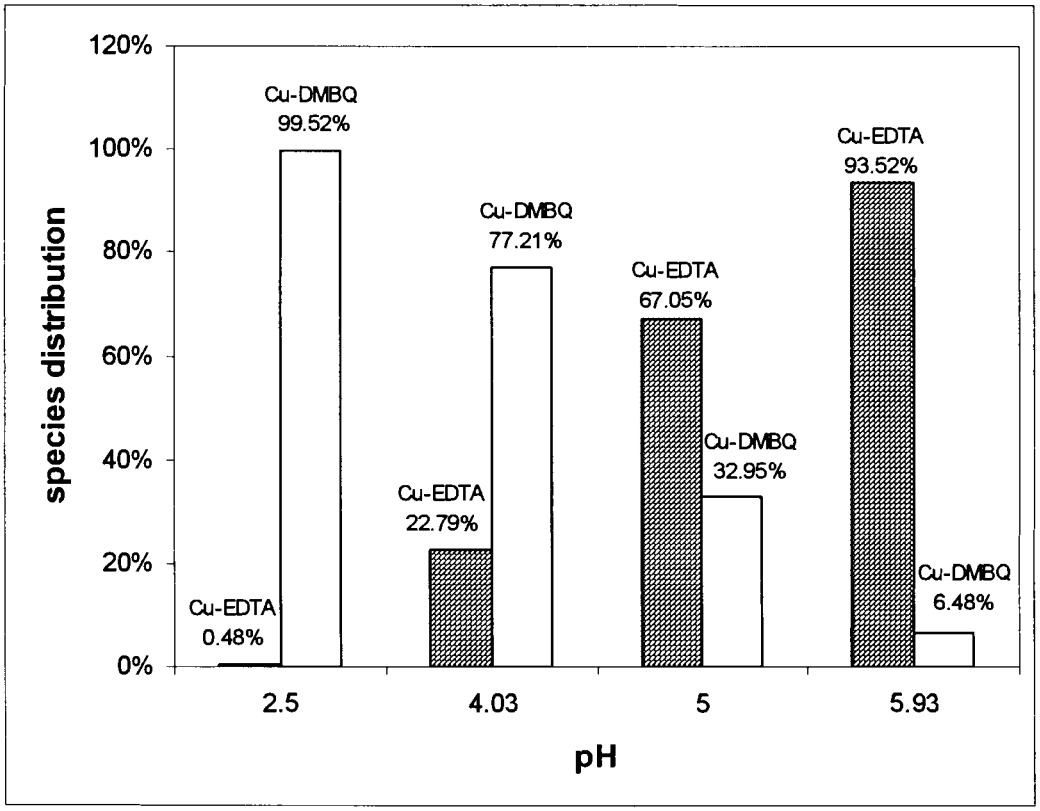

Figure 4.23: The species distribution of Cu at different pHs with 5×10^{-7}M Cu, 5×10^{-6} M EDTA and 2.5×10^{-5}M DMBQ at pH 2.5 and 4.03, 3.0×10^{-5}M DMBQ at pH 5.0 and 5.93.

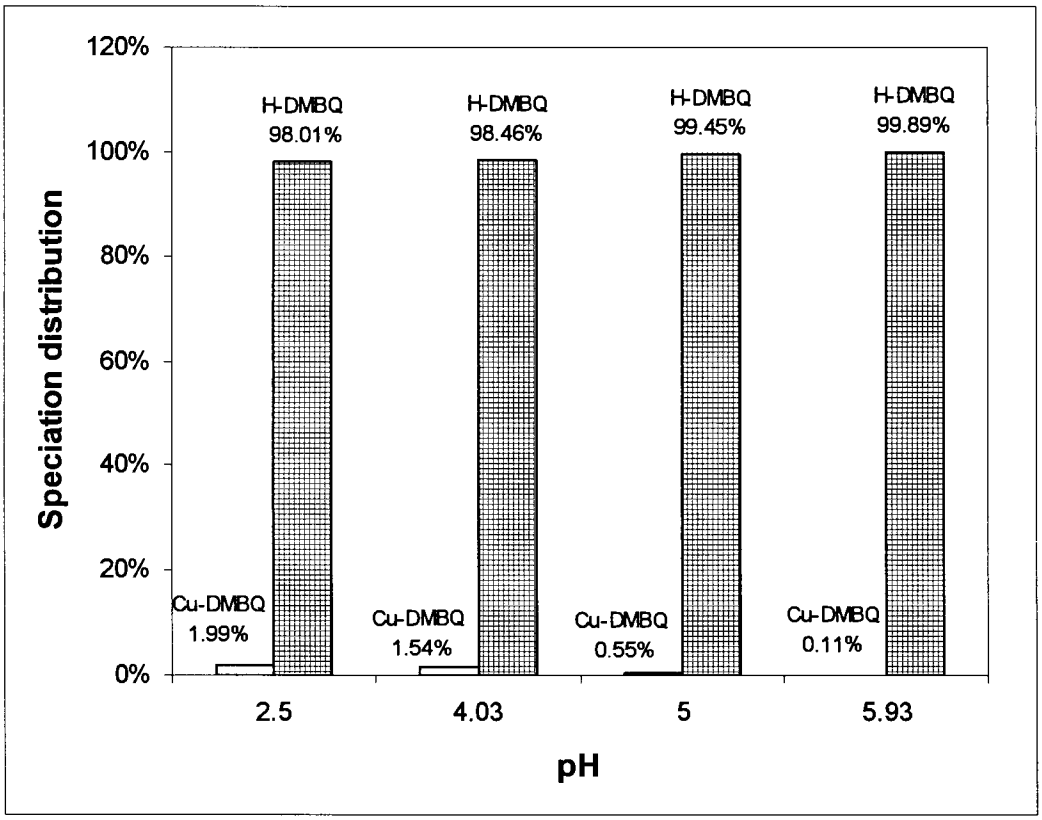

Figure 4.24: The speciation distribution of DMBQ at different pH with 5×10^{-7}M Cu, 5×10^{-6} M EDTA and 2.5×10^{-5}M DMBQ at pH 2.5 and 4.03, 3.0×10^{-5}M DMBQ at pH 5.0 and 5.93.

to reduce the pH, thus creating a pH gradient between the immediate fungal environment (pH≈2.5) and the wood cell wall (5.5-6.0)[5, 36]. Because oxalate is a weak chelator of transition metals (binding constants are shown in Table 4.4), Gt chelator has been proposed to sequester metals from it with the oxalate functioning as a phase transfer agent[36]. In Figure 4.25 the binding ability of 2,5-DMBQ to Cu(II) is compared with that of oxalic acid at different pHs. The Cu(II) distribution between 2,5-DMBQ and oxalic acid was calculated using MICROQL with the stability constants reported in Table 4.3 and Table 4.4. Due to the accumulation of oxalate surrounding the fungi hyphae[36], an excess of oxalic (2000 times) was used to do the speciation calculation.

Table 4.4: Dissociation reactions and related stability constants for transition metals and oxalic acid.

Dissociation reaction	Symbol	logK
$H_2Oxalic \leftrightarrow HOxalic^- + H^+$	K_1	1.25[64]
$HOxalic^- \leftrightarrow Oxalic^{2-} + H^+$	K_2	3.8[64]
$CuOxalic \leftrightarrow Cu^{2+} + Oxalic^{2-}$	β_{1Cu}	4.85[65]
$Cu(Oxalic)_2^{2-} \leftrightarrow Cu^{2+} + [Oxalic^{2-}]^2$	β_{2Cu}	10.23[65]
$FeOxalic^+ \leftrightarrow Fe^{3+} + Oxalic^{2-}$	β_{1Fe}	7.58[65]
$Fe(Oxalic)_2^- \leftrightarrow Fe^{3+} + [Oxalic^{2-}]^2$	β_{2Fe}	13.81[65]
$Fe(Oxalic)_3^{3-} \leftrightarrow Fe^{3+} + [Oxalic^{2-}]^3$	β_{3Fe}	18.6[65]

Figure 4.25 shows that 2,5-DMBQ is indeed a strong chelating reagent compared with oxalic acid at pH range from 2.5 to 6.0. Especially from pH 4.0 and up, 2,5-DMBQ is binding more Cu than oxalic acid even given a 1/2000 of DMBQ/oxalic ratio. Thus, the estimated stability constants of 2,5-DMBQ with Cu indicate that 2,5-DMBQ would be

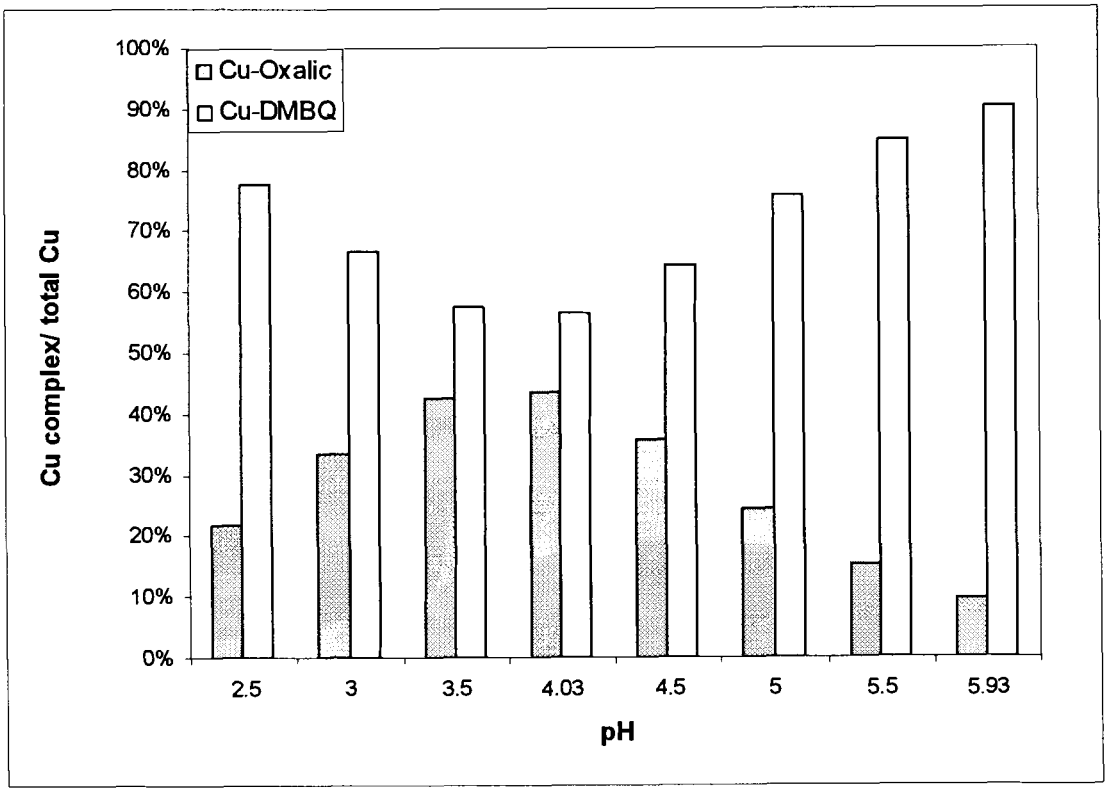

Figure 4.25: The species distribution of Cu at different pHs with 5×10^{-7}M Cu, 1×10^{-3} M Oxalic acid and 5×10^{-7}M DMBQ. In this work a 2000-fold greater concentration of oxalate was use compare to the DMBQ to simulate conditions that may occur in the fungal environment.

able to sequester Cu(II) from oxalic acid under conditions found in wood decay environments (pH=3-4). Further, the increasing affinity of the 2,5-DMBQ with increasing pH supports the data and hypothesis presented by Goodell et al[5, 36] with regard to phase transfer of transition metals as the pH increases from low immediately surrounding the fungal hyphae to much higher within the buffered environment of the wood cell wall. This is important as it suggests how reduced metals that can participate in Fenton reactions can be controlled so that damaging free radicals are prevented from forming in close proximity to the fungal hyphae whereas their generation is promoted in the higher pH environment within the wood cell wall. Due to the presence of trace amounts of iron in the environment of the laboratory, the binding ability of 2,5-DMBQ with Fe(III) could not be estimated by CLE/ASV method in this work. However, 2,5-DMBQ may have a stronger affinity with Fe(III) than Cu(II) like other organic ligands, such as salicylate and EDTA[65]. Thus, 2,5-DMBQ could sequester Fe(III) from oxalic acid in the wood decay conditions.

The study of binding affinity of cellulose and iron by Xu and Goodell[34] showed that the binding constant for cellulose-iron (about 10^5 M^{-1}) is smaller that that for Fe(III)-oxalate (10^8 M^{-1}), Fe(III)$(oxalate)_2$ (10^{14} M^{-1}), and Fe(III)$(oxalate)_3$ (10^{18} M^{-1}). Thus, the binding affinity of 2,5-DMBQ with iron should be greater than that of cellulose. This suggests that 2,5-DMBQ secreted by brown rot fungi may be capable of diffusing into the wood cell wall to sequester Fe(III) from cellulose to form Fe(III)-DMBQ complexes.

According to the work of Kerem et al[7], 2,5-dimethoxy-1,4-hydroquinone (2,5-DMHQ) and 2,5-DMBQ are produced by *G. trabeum* and they could undergo a quinone

redox cycle with Fe (III) to generate extracellular Fenton reagents Fe(II) and hydrogen peroxide (H_2O_2), which is responsible for biodegradation by brown rot fungi. However, in this quinone redox cycle process, reductase enzymes are needed to reduce 2,5-DMBQ to 2,5-DMHQ allowing the chelators to be cycled[6, 7]. But the quinone reductase or other enzymes are too large to penetrate the wood cell wall, it is unlikely that this mechanism functions to actively cycle quinones for continued metal reducing activity in the brown-rot decay process. Filley et al[67] proposed a hypothesis that, if a nonenzymatic quinone-driven Fenton's reaction is active within the wood cell wall, ferric iron and hydroxyl radicals are free to react with lignin and cellulose simultaneously where spatial considerations permit. Demethylation of lignin could be occurred by reaction with ferric iron and halides. It is possible that once a portion of the lignin is demethylated, the altered lignin backbone itself acts as a chelator and electron source for ferric/ferrous conversion. Thus, the fugal chelators would only need to be produced initially and in small amounts and afterward, the catechol/quinone-ferric/ferrous conversion would develop as a reaction front moving progressively through the lignin backbone. However, further experimental study needed to test this hypothesis. Our study of 2,5-DMBQ binding ability indicates that 2,5-DMBQ may increase the availability of Fe(III) in the wood decay environments and allow participation in some sort of non-enzymatic redox cycle in brown-rot decay process.

The reduction rate of Cu(II) by hydroquinone and its derivatives is very fast[68] and it may not possible to estimate the stability constant of Cu(II)-DMHQ complexes. However, the weak binding of Cu(II) by the oxidation product, DMBQ (Figure 4.24), at least does not have the strong ability to compete with DMHQ to react with Cu(II). This finding

may also relate to the binding of Fe(III), and suggests that a reaction between DMHQ and Fe(III) should be favorable under the conditions found in wood decay environments.

4.2 Cyclic voltammetry study

Cyclic voltammetry was used to study the interaction characteristics of Cu(II) and 2,3-DHBA in the absence and presence of H_2O_2. Cu(II) instead of Fe(III) was chosen in this study due to the low solubility of Fe(III) even at low pH conditions. Analysis of the cyclic voltammograms, was intended to show the reaction mechanisms between Cu and 2,3-DHBA and the effect of H_2O_2 upon these reaction mechanisms.

4.2.1 Cyclic voltammetric analysis of 2,3-DHBA

The electrochemical behavior of 2,3-DHBA was studied in aqueous solution under anoxic conditions at various pHs. Figure 4.26 illustrates the cyclic voltammograms of 2,3-DHBA at four different pHs. The anodic peaks A and B in each voltammogram represent the oxidation of 2,3-DHBA into the 'semiquinone' and the 'quinone' forms of the ligand, respectively[59, 60]. The oxidation to the quinone form occurring at the surface of the glassy carbon electrode is irreversible, because no corresponding reduction peak of the oxidation peak B appeared. The cathodic peak C in each voltammogram may represent the reduction of the semiquinone form back to the original ligand form. The cathodic peak D, was not identified in this work.

The potential of peak A varies with pH as shown in Table 4.5. This potential shift may be attributed to the speciation of 2,3-DHBA species in aqueous solution as a function of pH. Oxidation of 2,3-DHBA takes place more readily at high pH values, since the oxidation peaks A and B shift to a less positive potential as the pH increases. The

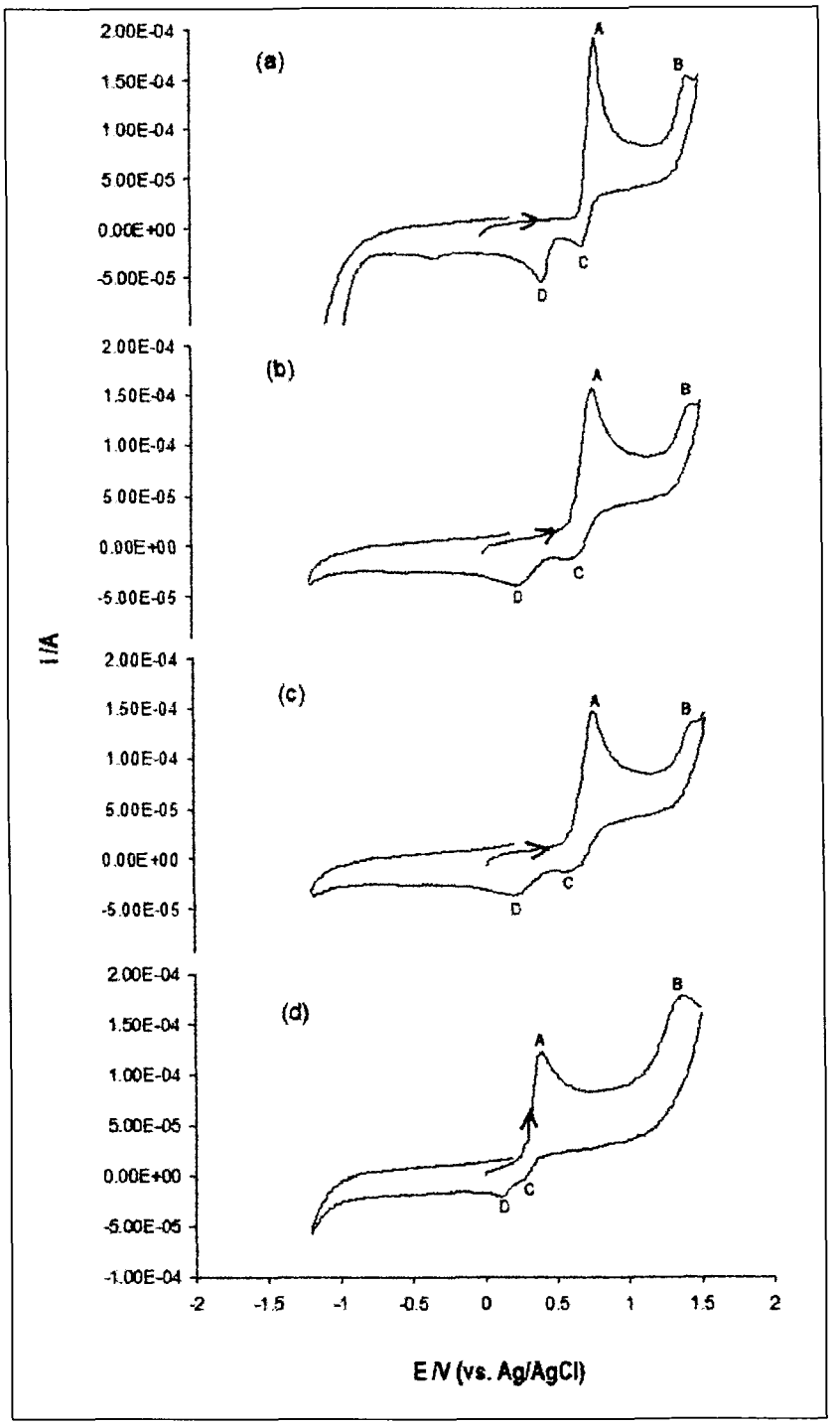

Figure 4.26: Cyclic Voltammograms for 5mM 2,3-DHBA in 0.5M KNO_3: (a) pH=2; (b) pH=4.4; (c) pH=7; (d) pH=12. Scan rate 0.5V/s (A: oxidation peak of DHBA to semiquinone; B: oxidation peak of semiquinone to quinone, C: reduction peak of semiquinone to DHBA; D: unknown).

Table 4.5: Cyclic voltammetry analysis data of 2,3-DHBA from Figure 4.26.

pH	Peak A		Peak B		Peak C		Potential Separation
	Potential (mV)	Current (uA)	Potential (mV)	Current (uA)	Potential (mV)	Current (uA)	E_{pa}-E_{pc} (mV)
2	790	189.93	1420	150.6	690	-18.15	100
4.4	760	156.46	1430	139.39	610	-13.69	150
7	660	154.99	1330	137.45	570	-12.33	90
12	400	121.68	1380	178.12	260	-6.07	140

height of the anodic peak A decreases in the order: pH2 > pH4.4 ≈ pH7> pH12, which indicates that semiquinone formation is favored at low pH[59].

The large oxidation-reduction peak potential separation between peaks A and C, as shown as (E_{pa}-E_{pc}) in Table 4.5, can be observed in all the voltammograms in Figure 4.26. This indicates that the electro-oxidation of 2,3-DHBA ligands is kinetically slow[69], since for a fully reversible reaction, this separation must be close to 59/n mV (n is the number of electrons transferred during the oxidation or reduction reaction) at 25°C[70]. The height of peak C is much smaller than that of peak A for each voltammograms in Figure 4.26. This quasi-reversible process may be attributed to the redox kinetics behavior between 2,3-DHBA and its semiquinone species[59]. The further oxidation of semiquinone to quinone species is an 'EC' mechanism[58], which is indicated by the oxidation peak B and no corresponding reduction peak. Oxidation from the semiquinone radical to its di-radical form is an electron transfer process at the surface of the electrode known as the 'E' mechanism, which is followed by a chemical process from the di-radical form to the quinone in solution (the 'C' mechanism). No reduction peak

appears even at very fast scan rates indicating that the di-radical form is very short-lived and turns into the quinone very quickly. The overall redox reaction scheme of 2,3,-DHBA at the surface of the electrode is shown in Figure 4.27.

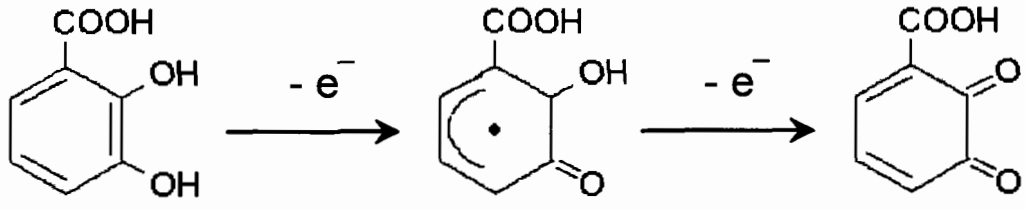

Figure 4.27: The redox reaction scheme of 2,3-DHBA

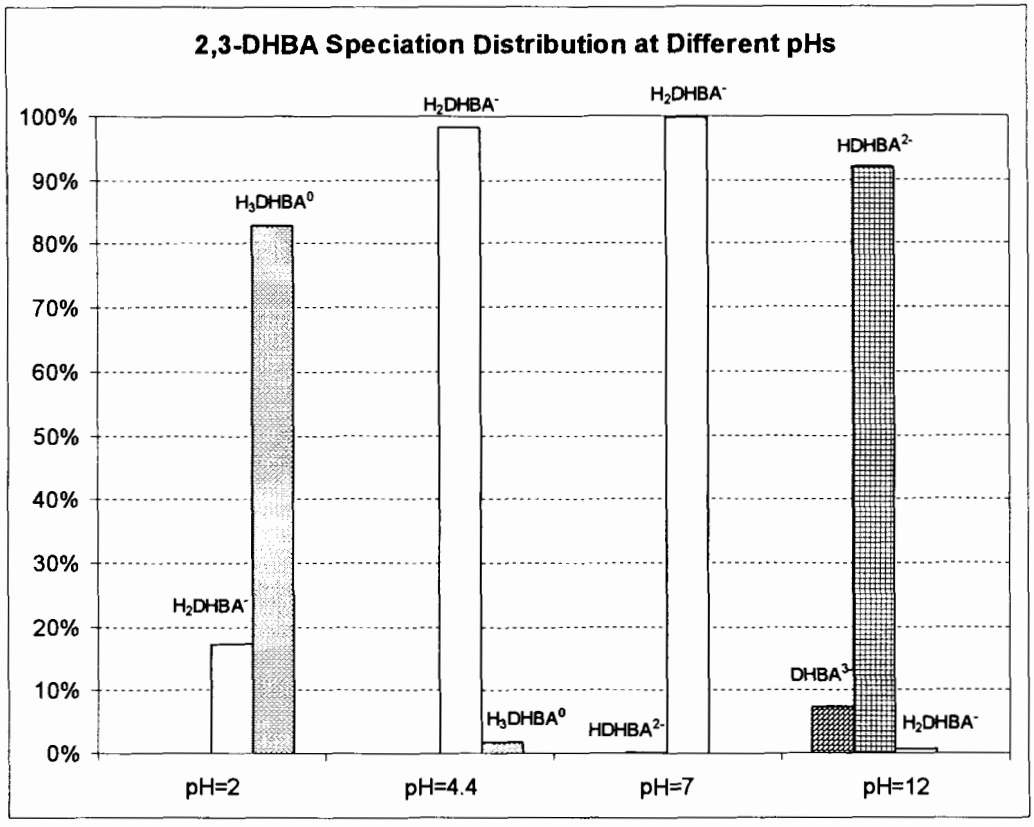

Figure 4.28: Speciation distribution of 5mM 2,3-DHBA in water at different pHs.

Figure 4.28 illustrates the species distribution of 5mM 2,3-DHBA in aqueous solution at different pHs, which was calculated by the MICROQL program. There are four species of 2,3-DHBA in aqueous solution. These are the fully protonated species H_3DHBA^0, partially protonated species H_2DHBA^- and $HDHBA^{2-}$, and fully deprotonated species $DHBA^{3-}$. The dissociation reactions among these four species and their acidity constants are shown in Table 4.6. Figure 4.28 shows that at pH 2, fully protonated H_3DHBA^0 is the dominant species in aqueous solution, at pH 4.4 and 7, H_2DHBA^- is the dominant species, and at pH 12, $HDHBA^{2-}$ is the dominant species.

Table 4.6: Dissociation reactions and related acidity constants for 2,3-DHBA.

Dissociation reactions	pK_a [71]
$H_3DHBA^0 \leftrightarrow H_2DHBA^- + H^+$	2.68
$H_2DHBA^- \leftrightarrow HDHBA^{2-} + H^+$	9.84
$HDHBA^{2-} \leftrightarrow DHBA^{3-} + H^+$	13.1

As discussed previously, oxidation of 2,3-DHBA at the surface of the electrode was facilitated as the pH increased. This can be explained by the different species distribution of 2,3-DHBA. At a high pH (such as pH 12), the dominant monoprotonated $HDHBA^{2-}$ species has a higher electron density than the fully protonated H_3DHBA^0 species and the diprotonated H_2DHBA^- species. Thus, the $HDHBA^{2-}$ species is oxidized at a less positive potential than the other two species. At pH 2, the dominant species is H_3DHBA^0, which has three protons and a lower electron density, and thus, it is the most stable species against oxidation. At pH 4.4 and 7, the dominant species is H_2DHBA^-, which is oxidized at a potential between those of H_3DHBA^0 and $HDHBA^{2-}$.

4.2.2 Cyclic voltammetric study of Cu(II) and 2,3-DHBA

Cyclic voltammetric measurements were made in aqueous solutions, containing different ratios of Cu(II) to 2,3-DHBA at pH 4.4. Figure 4.29 illustrates a cyclic voltammogram with a 10:1 ratio of Cu(II)/2,3-DHBA, which is compared with a voltammogram for 2,3-DHBA only.

As before, the anodic peaks A and B in the cyclic voltammograms are attributed to the oxidation of free 2,3-DHBA species and Cu(II)-DHBA complexes to the semiquinone and quinone forms, respectively. The cathodic peak C is assigned to reduction of semiquinone back to the original ligand.

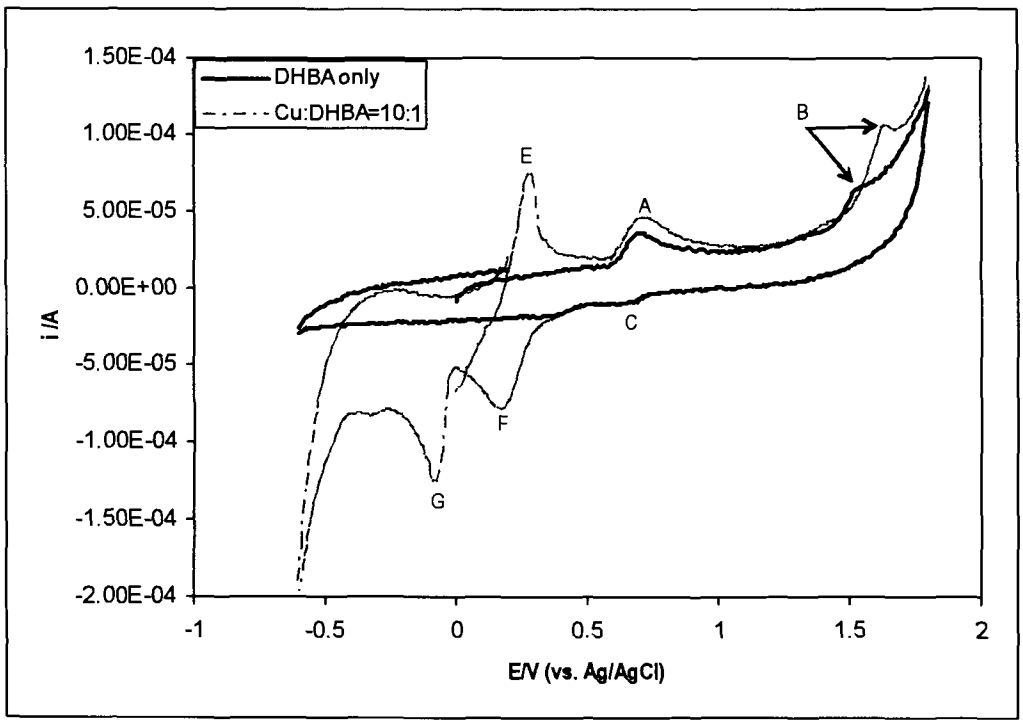

Figure 4.29: Cyclic Voltammograms at pH=4.4: 5mM Cu with 0.5mM DHBA and 0.5mM DHBA only (Scan rate 0.5V/s; supporting electrolyte 0.5M KNO_3) (A, B, C as indicated in Figure 4.26, E: oxidation peak of Cu(I) to Cu(II); F: reduction peak of Cu(II) to Cu(I) and G: reduction peak of Cu(I) to Cu(0)).

When Cu (II) is analyzed alone, peaks E, F and G appear in the voltammogram (not shown in Figure 4.29). These peaks increase with increased Cu concentration. The anodic peak E may be assigned to the oxidation of Cu(I) to Cu(II). Although there is no Cu(I) in solution originally, some Cu(I) may be produced at the surface of electrode when the voltammetric scan is initiated at 0V. Peak F may be assigned to the reduction of Cu(II) to Cu(I), and Peak G may be assigned to the reduction peak of Cu(I) to Cu(0). The data for peaks B, E, F and G with different Cu/DHBA ratios are shown in Table 4.7.

The presence of Cu increases the anodic current of the semiquinone/quinone couple (peak B) as shown in Table 4.7 and Figure 4.30. The effect of Cu on the anodic peak of semiquinone/quinone can be explained as follows, and as illustrated in Figure 4.31: 2,3-DHBA is oxidized to its quinone form by two one-electron-transfer steps (2,3-DHBA to semiquinone radical and semiquinone radical to quinone) at the surface of the electrode. At the same time, Cu(II) oxidizes 2,3-DHBA into its semiquinone radical in the bulk solution[72]. This semiquinone radical diffuses to the surface of the electrode where it is oxidized into the quinone form, resulting in an increase in the current compared to the oxidation of 2,3-DHBA at the surface of electrode in the absence of Cu(II). The height of peak B increases with Cu concentration in solution (Figure 4.32), which indicates that formation of the semiquinone radical is favored at high Cu concentrations. The overall process may be classified as a 'CE' mechanism, with the 'C' step representing the chemical reaction in the solution followed by the redox reaction involving the product at the surface of the electrode represented by the 'E' step:

$$C \text{ step}: \quad 2,3DHBA + Cu(II) \rightarrow Cu(II)\text{-}DHBA \underset{k_r}{\overset{k_f}{\leftrightarrow}} semiquinone\ radical + Cu(I) \quad (4\text{-}2)$$

$$E \text{ step}: \quad semiquinone\ radical - e^- \leftrightarrow quinone \quad (4\text{-}3)$$

Table 4.7: Cyclic voltammetry analysis data for different Cu/2,3-DHBA ratios.

Cu/DHBA ratios	Peak B		Peak E		Peak F		Peak G	
	Potential (mV)	Current (uA)	Potential (mV)	Current (uA)	Potential (mV)	Current (uA)	Potential (mV)	Current (uA)
DHBA only	1340	67.74	–	–	–	–	–	–
1:10	1370	77.84	–	–	–	–	–	–
1:5	1380	81.98	–	–	–	–	–	–
1:2	1400	86.73	250	11.2	–	–	–	–
1:1	1400	89.49	250	12.94	90	-28.28	-256	-32.00
2:1	1410	95.93	270	18.99	160	-33.00	-160	-41.95
5:1	1420	105.25	250	23.95	150	-51.44	-110	-71.35
10:1	1450	111.33	280	73.03	170	-77.90	-80	-124.3
Cu only	–	–	300	99.80	160	-59.28	-90	-86.71

There are no theoretical treatments for the voltammetric reactions involving the 'CE' mechanism such that the reaction rate constant may be directly calculated from the experimental data[58]. Theoretical treatment of this data is further complicated by the fact that Cu(II) is continually regenerated due to the oxidation of Cu(I) at the surface of electrode for potentials above 0 V.

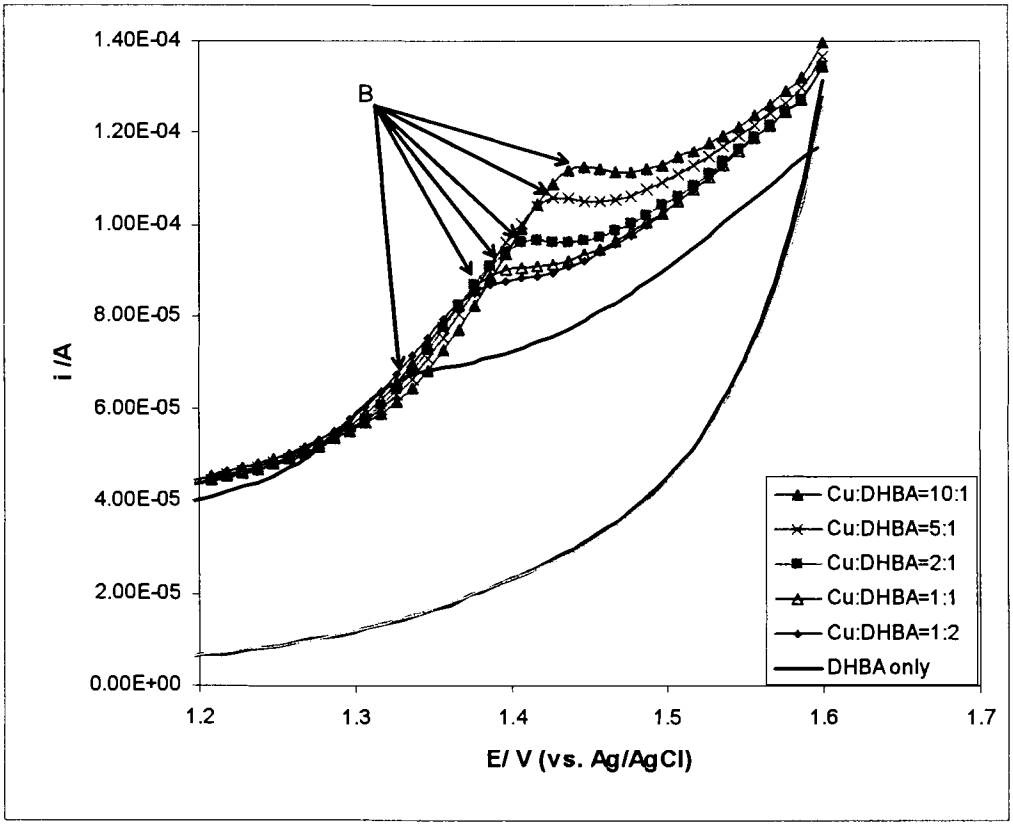

Figure 4.30: Voltammograms of anodic peak B with different Cu/DHBA ratios at pH 4.4, 0.5mM 2,3-DHBA (The height of peak indicates the concentration of semiquinone) (scan rate 500mV/s, 0.5M KNO_3).

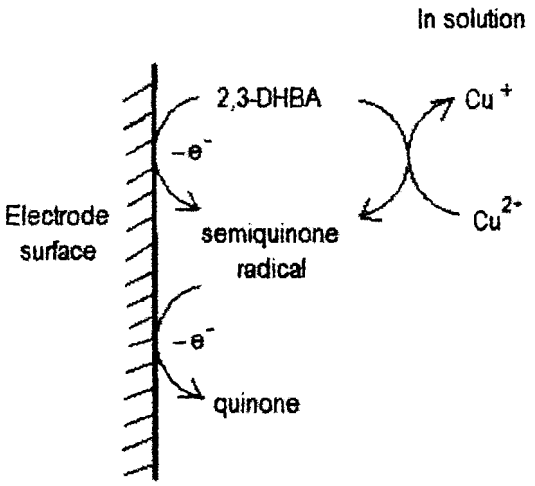

Figure 4.31: Redox scheme of Cu-DHBA complex at pH 4.4.

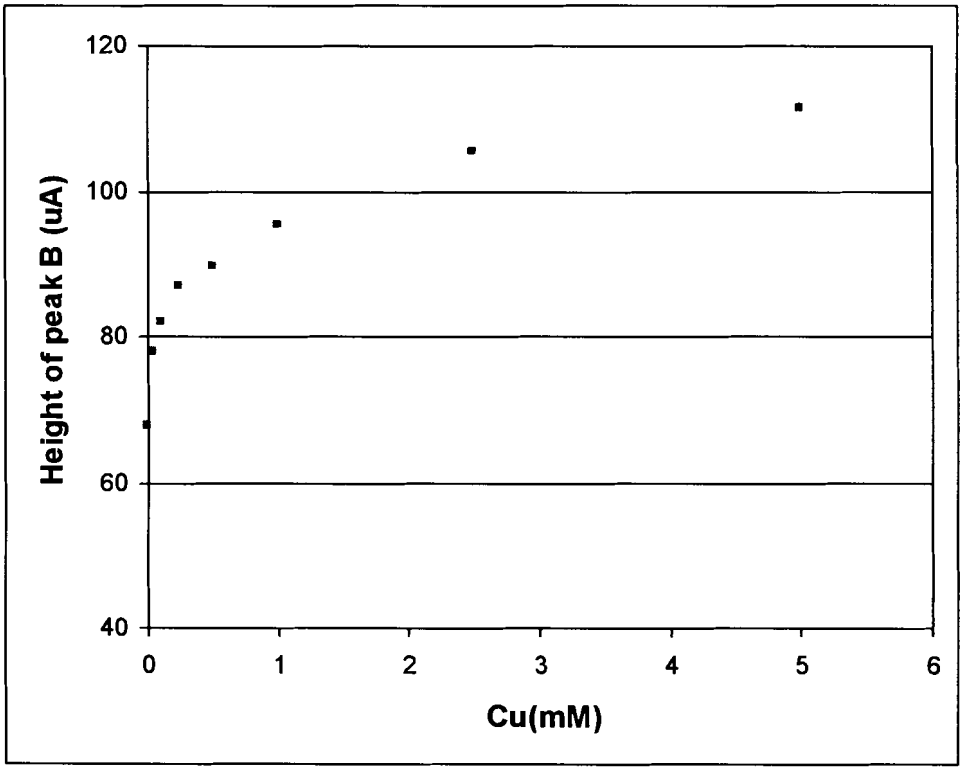

Figure 4.32: Current height of peak B increases with Cu concentration for 0.5mM 2,3-DHBA concentration at pH 4.4 with the scan rate 0.5V/s. (The height of peak B indicates the concentration of semiquinone).

The scheme for the reaction in equation 4-2 may be described as in Figure 4.33:

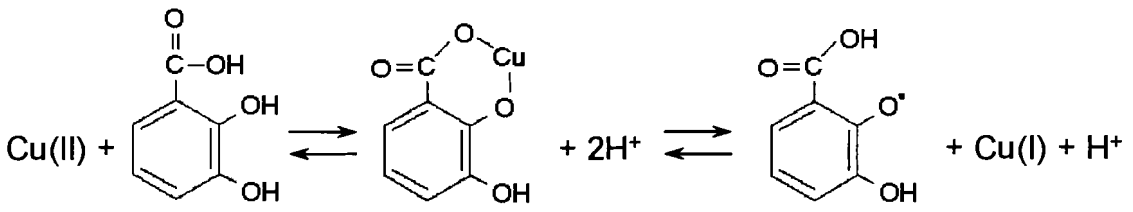

Figure 4.33: The scheme of interaction between Cu and 2,3-DHBA.

The initial step in the oxidation of 2,3-DHBA by Cu(II) involves the formation of a Cu(II)-DHBA complex. The next step may involve intramolecular electron transfer within the Cu(II)-DHBA complex to produce Cu(I) and the DHBA radical. The formation of the initial Cu-DHBA complex likely alters the electron density distribution increasing the probability that the semiquinone can form by one electron oxidation with Cu[5]. The semiquinone structure is then further oxidized at the surface of working electrode to form the quinone species.

Alternatively, it may be possible, in analogy to Xu and Jordan's observation for the oxidation of 2,3-DHBA by Fe(III)[73], that the Cu(II)-DHBA complex is subsequently oxidized by an additional Cu(II) to form the semiquinone intermediate with the concurrent reduction of only the second Cu(II) to Cu(I). However, at least in the presence of an excess of 2,3-DHBA, involvement of a second Cu(II) in the oxidation of 2,3,-DHBA by Cu(II) may not be likely due to the lack of Cu(II) available. Ferrozine assay results with iron and 2,3 DHBA have confirmed that an excess of 2,3-DHBA may indeed inhibit Fe(III) reduction[74]. This inhibition effect of Fe(III) reduction probably because the hexadentate coordination of 2,3-DHBA with iron, which ties up the iron preventing

further reaction. However, Cu (II) could not have the hexadentate coordination with 2,3-DHBA. In the cyclic voltammetric study, the formation of semiquinone is not inhibited by an excess concentration of 2,3-DHBA with respect to Cu(II). As shown in Figure 4.30 and 4.32, the height of peak B increases with Cu(II) concentration even at low Cu(II)/2,3-DHBA ratios down to 10:1. According to the observations of this cyclic voltammetry study, in contrast to Xu and Jordan's observations for the oxidation of 2,3-DHBA with Fe(III) where a second Fe(III) is required, the presence of a second Cu(II) does not appear to be required for the oxidation of 2,3-DHBA by Cu(II) for the concentration range used here.

4.2.3 Cyclic voltammetric study of Cu(II), 2,3-DHBA and hydrogen peroxide (H_2O_2)

4.2.3.1 CV study of Cu(II) and H_2O_2 at pH 4.4

Cyclic voltammetric measurements were made in aqueous solutions, containing different ratios of Cu(II) to H_2O_2 at pH 4.4. Figure 4.34 shows the voltammograms of Cu(II) with different concentrations of H_2O_2. Solutions containing only H_2O_2 do not exhibit any peaks within the voltammetric scan range used here. Peaks F and G are assigned to the reduction of Cu(II) to Cu(I), and Cu(I) to Cu(0), respectively. In the presence of H_2O_2, peak G, which was assigned to the reduction of Cu(I) to Cu(0) at the surface of the electrode, decreases due to the oxidation of Cu(I) to Cu(II) by H_2O_2 and possibly by $OH^{\bullet}$ as indicated by equations 4-4 and 4-5.

$$H_2O_2 + Cu(I) + H^+ \rightarrow OH^{\bullet} + Cu(II) + H_2O \qquad (4\text{-}4)$$

$$OH^{\bullet} + Cu(I) + H^+ \rightarrow Cu(II) + H_2O \qquad (4\text{-}5)$$

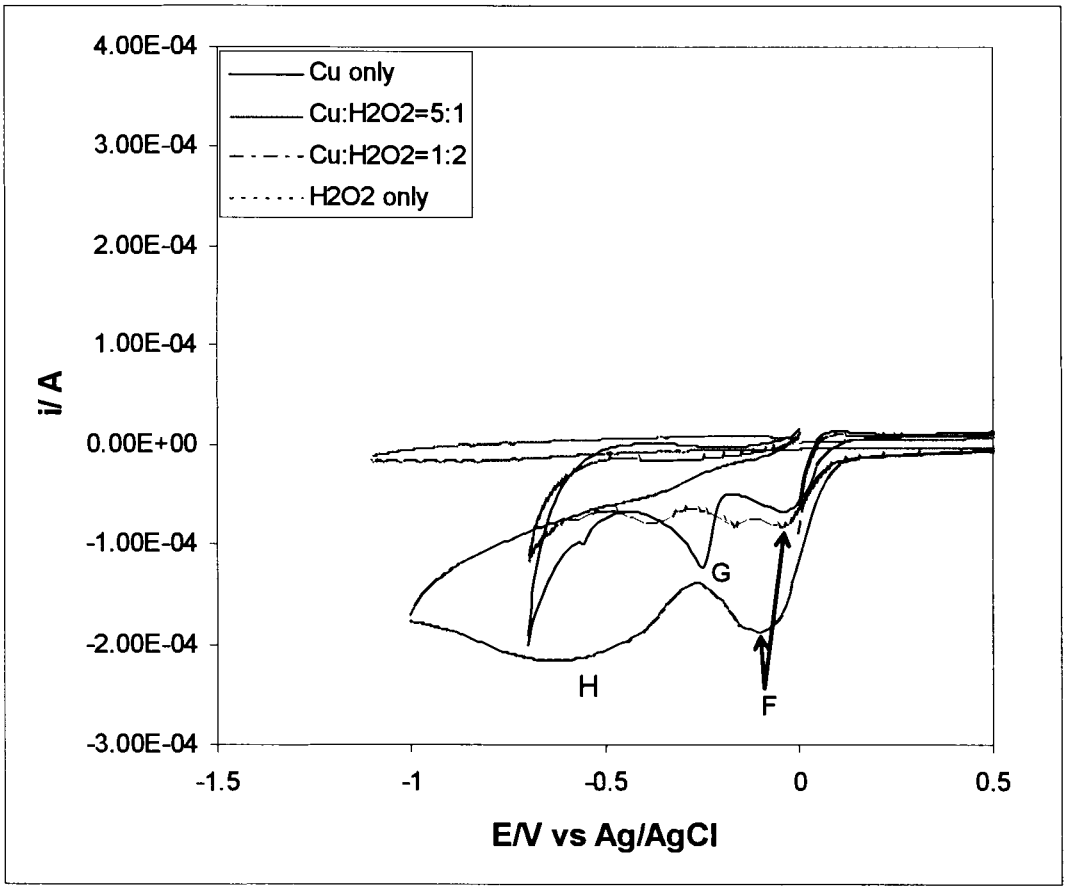

Figure 4.34: Voltammograms of 5mM Cu, 5mM Cu and 1mM H_2O_2, 5mM Cu and 10mM H_2O_2, and 5mM H_2O_2 at pH 4.4 (scan rate 0.5V/s, in 0.5M KNO_3) (peak F and G as indicated in Figure 4.29; H: the reduction peak of O_2).

Peak F, which was assigned to the reduction of Cu(II) to Cu(I) at the surface of the electrode, however, increases with H_2O_2 concentration due to the increase in the concentration of Cu(II) brought about by the oxidation of Cu(I) to Cu(II) by H_2O_2 and $OH^{\bullet}$ in solution.

For a 1:2 ratio of Cu/H_2O_2, a new peak H appears. This peak may be assigned to the reduction of dioxygen (O_2) at the surface of electrode as established separately by conducting voltammetric scans of an electrolyte solution saturated with O_2. Peak H is absent when Cu(II)/H_2O_2>1. Therefore, we propose that the following reactions may be dominant[75] instead of reaction 4-5 when Cu(II)/H_2O_2<1.

$$H_2O_2 + OH^{\bullet} \rightarrow HOO^{\bullet} + H_2O \leftrightarrow O_2^{\bullet -} + H^+ \quad (4\text{-}6)$$

$$Cu(II) + O_2^{\bullet -} \rightarrow Cu(I) + O_2 \quad (4\text{-}7)$$

$$Cu(II) + HOO^{\bullet} \rightarrow Cu(I) + O_2 + H^+ \quad (4\text{-}8)$$

A similar behavior has also been proposed for the reactions involving different concentrations of Fe and H_2O_2[76].

4.2.3.2 CV study of Cu(II), 2,3-DHBA and H_2O_2 at pH 4.4

Cyclic voltammetric measurements were made in aqueous solutions, containing constant concentrations of Cu(II) and 2,3-DHBA with different concentrations of H_2O_2 at pH 4.4. Figure 4.35 illustrates the cyclic voltammograms of 2,3-DHBA only, Cu-2,3-DHBA, and Cu-2,3-DHBA-H_2O_2 at pH 4.4. The analysis data are given in Table 4.8.

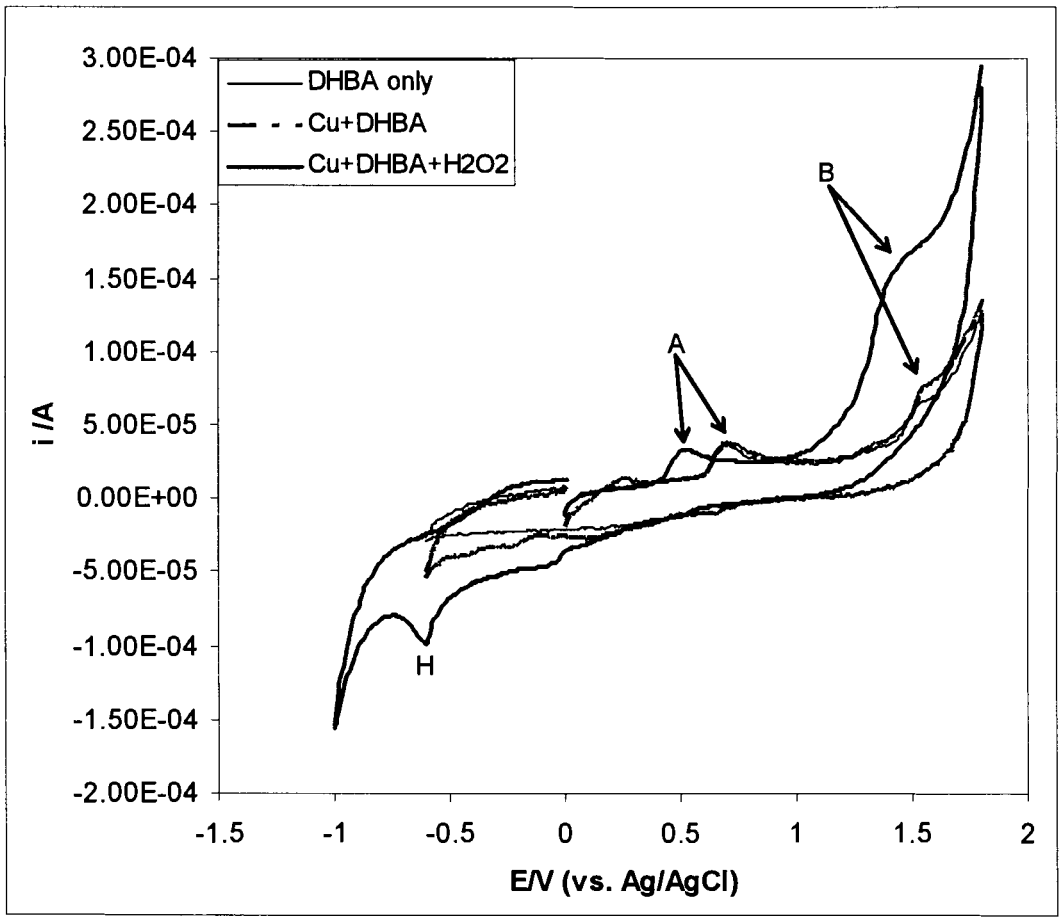

Figure 4.35: Voltammograms of 0.5mM 2,3-DHBA, 0.5mM Cu+0.5mM 2,3-DHBA and 0.5mM Cu+0.5mM 2,3-DHBA+2.5mM H_2O_2 at pH4.4 (Scan rate 0.5V/s, 0.5M KNO_3) (Peak A and B as indicated in Figure 4.26; Peak H as indicated in Figure 4.34).

Table 4.8: Cyclic voltammetry analysis data for Figure 4.35.

	Peak A		Peak B		Peak H	
	Potential (mV)	Current (uA)	Potential (mV)	Current (uA)	Potential (mV)	Current (uA)
DHBA only	710	35.81	1540	66.15	–	–
Cu and DHBA	700	37.27	1560	76.51	–	–
Cu, DHBA and H_2O_2	520	31.53	1410	150.5	-600	-100.28

The anodic peak A in Figure 4.35 was assigned to the oxidation of Cu(II)-DHBA complexes and free 2,3-DHBA into semiquinone as before. In the presence of H_2O_2, this oxidation is more favored since it occurs at a less positive potential compared to absence of H_2O_2. The anodic current of the semiquinone/quinone couple (peak B) also increases nearly two fold in the presence of H_2O_2. Peak H due to the reduction of O_2 is generated only in the presence of H_2O_2. For constant concentrations of Cu(II) and 2,3-DHBA , both the anodic peak B and cathodic peak H increase with an increase in hydrogen peroxide concentration as shown in Figure 4.36 and Table 4.9.

The mechanism for the increase of peak B in the presence of H_2O_2 can be described as follows:

At the surface of the electrode, 2,3-DHBA is oxidized to semiquinone and quinone forms as described in equation 4-3. In solution, Cu(II) reacts with DHBA and H_2O_2 as described as equations 4-2 and 4-4, respectively. Equation 4-4 is a Fenton type reaction which

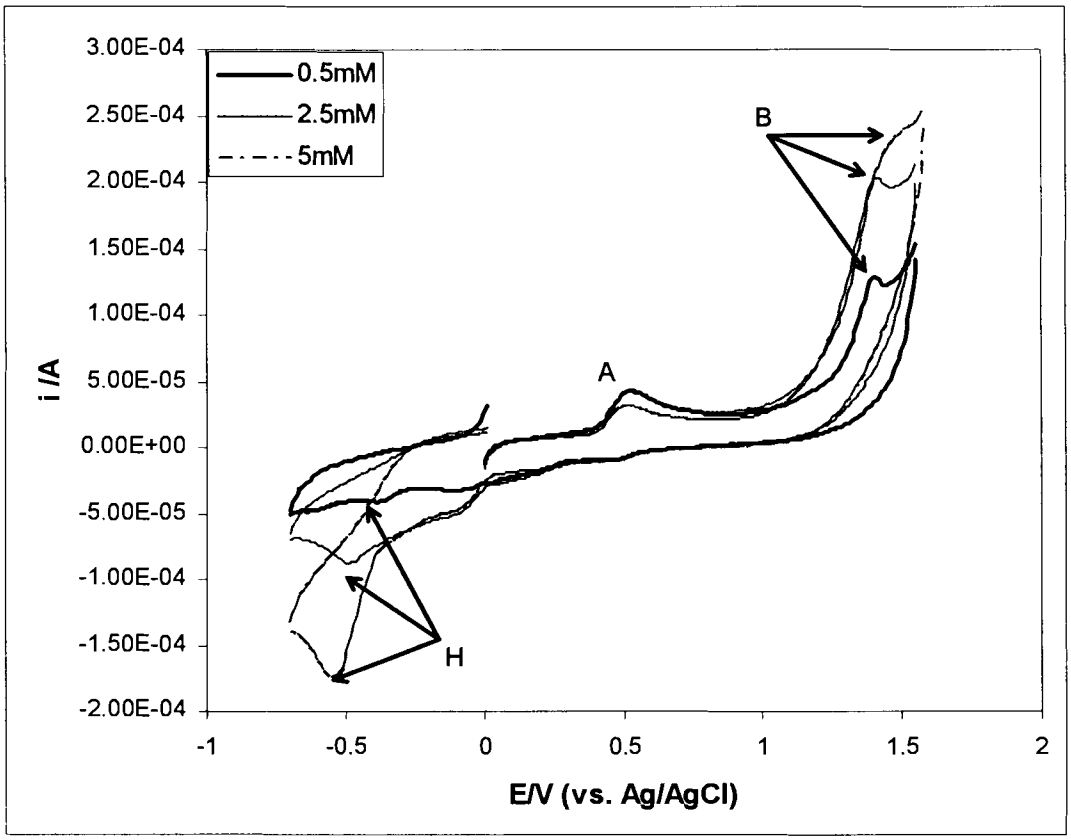

Figure 4.36: Voltammograms of 0.5mM Cu and 0.5mM 2,3-DHBA with different concentrations of H_2O_2 at pH 4.4 (scan rate 0.5V/s, in 0.5M KNO_3) (Peak A and B as indicated in Figure 4.26; peak H as indicated in Figure 4.34).

Table 4.9: Cyclic voltammetry analysis data for Figure 4.36.

H_2O_2 (mM)	Peak A		Peak B		Peak H	
	Potential (mV)	Current (uA)	Potential (mV)	Current (uA)	Potential (mV)	Current (uA)
0.5	530	42.51	1400	128.66	-370	-41.48
2.5	520	42.87	1410	201.75	-490	-87.56
5	500	32.23			-550	-172.88

forms highly reactive $OH^{\bullet}$. The $OH^{\bullet}$ can then attack either Cu(II) (equation 4-5) or DHBA as shown below:

$$OH^{\bullet} + DHBA + H^{+} \rightarrow semiquinone\ radical + H_2O \quad (4\text{-}9)$$

$$OH^{\bullet} + semiquinone\ radical + H^{+} \rightarrow quinone + H_2O \quad (4\text{-}10)$$

The presence of H_2O_2 generates more semiquinone radicals than in the absence of H_2O_2. This is primarily due to the fact that Cu acts as a catalyst in the Fenton reaction to oxidize DHBA (equations 4-2 and 4-4). This results in an increase of the anodic current for the semiquinone/quinone couple.

In presence of H_2O_2, the $OH^{\bullet}$ generated by the reaction of H_2O_2 and Cu(I) can either attack 2,3-DHBA to form the semiquinone species directly, or attack H_2O_2 to form $HOO^{\bullet}$ and $O_2^{\bullet-}$, which in turn reduces Cu(II) to Cu(I). This redox cycling continually generates the semiquinone radical species, which could be indicated by the increase of peak B in the voltammograms. In the presence of excess H_2O_2, the overall process forms the redox cycling as described in Figure 4.37.

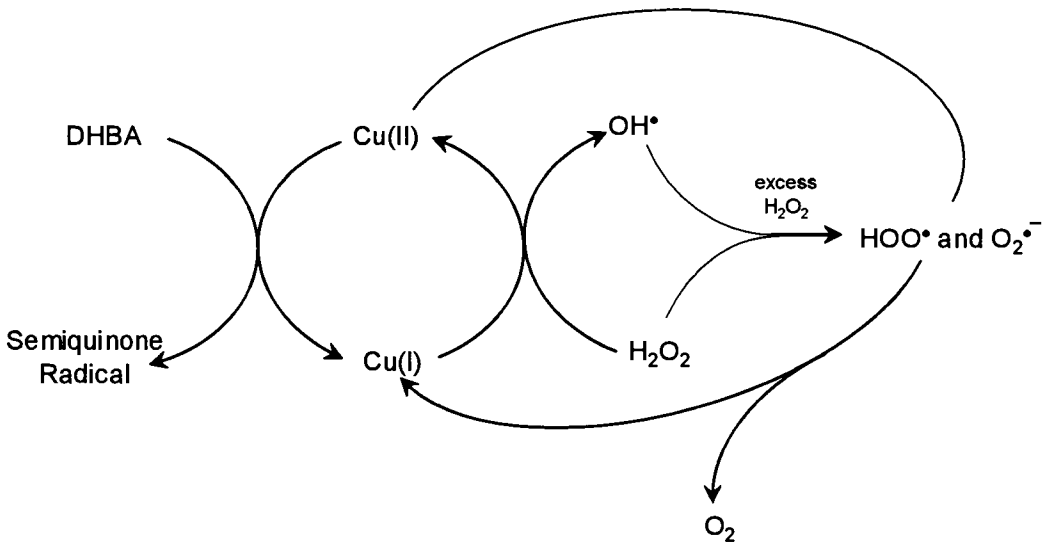

Figure 4.37: The redox cycling scheme of Cu-2,3-DHBA-H_2O_2 system.

The cyclic voltammetry study on 2,3-DHBA itself shows that the electrochemical oxidation of 2,3-DHBA to its semiquinone form becomes easier as the pH increases. This indicates that the reducing ability of 2,3-DHBA is greater at high pH. This may provide an explanation to the question of why iron reduction by Gt chelator is favored at pH 4.0 or greater, in contrast to low pH environments.[34]. Oxalate produced by brown rot fungi has been proposed to function in the control of pH of the fungal environment, which creating a pH gradient between the immediate fungal environment (pH≈2.5) and the wood cell wall (5.5-6.0)[5, 36]. The redox reaction between a transition metal and 2,3-DHBA or Gt chelator is favorable in the wood cell wall (higher pH). Thus, the hydroxyl radicals produced by the chelator-mediated Fenton system would also favorable in the wood cell wall, the region undergoing degradation.

The cyclic voltammetric study with Cu(II) and 2,3-DHBA shows that Cu(II) can oxidize 2,3-DHBA to its semiquinone form under acidic conditions, similarly to the oxidation action reported by Fe(III)[5, 34]. the cyclic voltammetry study on Cu(II), 2,3-DHBA and H_2O_2 shows that Cu(II) can also react with dihydroxy derivatives (such as 2,3-DHBA) at low pH conditions to drive the Fenton chemistry reactions to generate $OH^{\bullet}$. In the presence of 2,3-DHBA, the Fenton-type reaction between Cu(I) and H_2O_2 is accelerated due to continual generation of Cu(I), not only from the reaction between Cu(II) with $HOO^{\bullet}$ and $O_2^{\bullet -}$, but also because of reduction of Cu(II) by 2,3-DHBA. Thus more hydroxyl radical will be produced than would be expected than from Fenton chemistry alone. This is consistent with studies of hydroxyl radical activity by Qian et al[37], in which hydroxyl radicals are produced by Fe(II) and H_2O_2 and where radical production or activity occurs over a longer time span when in the presence of 2,3-DHBA

than in the absence of 2,3-DHBA. Fe(III) may undergo the same reaction mechanisms with 2,3-DHBA and H_2O_2 as Cu (II) as shown in Figure 4.37. In this case, in the fungal decay environment, as proposed by Kerem et al.[7], O_2 could react with DHMQ semiquinone to produce H_2O_2 and DMBQ, which forms the cycle between H_2O_2 and O_2. This may provide a possible source of H_2O_2 in the wood cell wall. Thus, the production of hydroxyl radicals could occur in the wood cell wall with available Fenton reagents, H_2O_2 and Fe(II) (from reduction of Fe(III) by the chelator).

The cyclic voltammetry analysis with Cu(II) and 2,3-DHBA did not provide an explanation of how is quinone may be reduced to hydroquinone in the wood decay process to potentially maintain the cycle of a 'chelator-mediated' Fenton chemistry. During the voltammetry scan, quinone and semiquinone radicals of 2,3-DHBA were reduced on the surface electrode. No evidence indicated Cu or H_2O_2 was involved in these reductions. Other types of study may be needed to elucidate the hypothesized reduction of quinone via a nonenzymatic mechanism in wood decay processes.

In this work, direct study Fe(III) with 2,3-DHBA using cyclic voltammetry techniques was not possible due to the low solubility of Fe(III) even at low pH conditions. In the cyclic voltammetry study, given the available environment and instrumentation, a minimal 0.5mM concentration of Fe(III) was required to obtain acceptable voltammograms and to perform related analyses on the redox mechanisms of Fe(III). Thus, a very low pH condition (<1) could have been used to solubilize 0.5mM Fe(III) for the analysis. This is a lower pH than would normally occur in the natural fungal environment, and the data obtained would therefore have been of little value fro this study. Alternatively, oxalic acid could have been added to increase the solubility of Fe(III)

at a higher pH, such as pH 4. This could also be useful in mimicking the wood decay environment. However, oxalic acid itself may have oxidation and reduction peaks during the voltammetric scan. Thus, a more complicated voltammogram will be obtained in the presence of oxalic acid. This may increase the difficulty of analyzing the reaction system and complicate peak assignments for specific oxidation or reduction reactions.

Future work could also be done with Cu(II) or Fe(III) and 2,5-DMBQ using the cyclic voltammetry technique. Future work in this area may allow a reaction mechanism between metals and 2,5-DMBQ to be proposed through the analysis of voltammograms as outlined in this work.

CHAPTER 5

CONCLUSIONS

5.1 Ligand exchange study

The results of a competitive ligand exchange study for the Cu, 2,5-dimethoxybenzoquinone (2,5-DMBQ) system show that there are two possible species formed at a pH range between 4.0 and 6.9, $CuDMBQ^{2+}$ and $HDMBQ^{+}$. The relevant equilibrium stability constants for the formation of these complexes estimated from experimental data by FITEQL[63] program are 22.52 and 15.94, respectively. Speciation analysis using these stability constants shows that 2,5-DMBQ has a relatively strong binding ability with Cu(II) at low pH conditions. If these results can be assume to be similar to the reactions between 2,5-DMBQ with Fe (III), the strong binding affinity of 2,5-DMBQ would allow sequestration of Fe(III) from both oxalate and wood cell wall components, thus increasing the availability of Fe(III) in the wood decay process. Under acidic conditions, most 2,5-DMBQ exists in the $HDMBQ^{+}$ form, which will not effectively compete with its reduced form, 2,5-dimethoxyhydroquinone to inhibit the quinone redox cycle.

5.2 Cyclic voltammetry study

From the cyclic voltammetry study in this work, it can be concluded that:

1. 2,3-DHBA is electrochemically oxidized to its semiquinone and quinone form via two one-electron transfer steps. Oxidation of 2,3-DHBA is facilitated as pH increased, which suggests that the redox reaction between the metal and 2,3-

DHBA may be more favorable in the wood cell wall (pH 4-6) rather than in the environment immediately adjacent to the fungal hyphae. This would therefore potentially allow the generation of $OH^{\bullet}$ radicals away from the fungus where they would be damaging, and permit production instead within the wood cell wall where oxidation of wood cell wall components would occur as part of the decay process.

2. In the presence of Cu(II), the overall oxidation process of 2,3-DHBA may be classified as a 'CE' mechanism. The increase of anodic current of the semiquinone/quinone couple with Cu(II) indicates that 2,3-DHBA is oxidized by Cu(II) in solution to generate the DHBA semiquinone radical (the 'C' step), followed by further oxidation of the semiquinone to the quinone at the surface of electrode (the 'E' step). This indicates that DHBA will be oxidized by Cu(II) under acidic conditions.
3. The increase of a cathodic peak due to the reduction of Cu(II) to Cu(I), and the decrease of the cathodic peak due to reduction of Cu(I) to Cu(0) in the presence of H_2O_2 suggest that Cu(II) can be regenerated via the Fenton reaction between Cu(I) and H_2O_2 under the experimental conditions. In the presence of excess H_2O_2, the $OH^{\bullet}$ produced from the oxidation of Cu(I) in solution is scavenged producing $HOO^{\bullet}$ and $O_2^{\bullet-}$ species. Further reaction of Cu(II) with the latter two species generates dissolved oxygen. This could provide a source of H_2O_2 in the wood cell wall via a reaction between O_2 and DMHQ.
4. The increase in the anodic current of the semiquinone/quinone couple in the presence of H_2O_2 indicates that DHBA semiquinone radicals are not only

generated from the electron transfer step at the surface electrode and the oxidation 2,3-DHBA by Cu(II), but also generated by oxidation of 2,3-DHBA by hydroxyl radicals ($OH^{\bullet}$). The redox cycle involving Cu(II), 2,3-DHBA and H_2O_2 leads to a continuous regeneration of Cu(II) and production of $OH^{\bullet}$, which accelerate the formation of DHBA semiquinone radicals. A proposed reaction mechanism from this study indicates that $OH^{\bullet}$ production by the Fenton reaction is accelerated by the reaction between Cu(II) and 2,3-DHBA.

In summary, the cyclic voltammetry study shows evidence that the chelator-mediated Fenton reaction is favored in the wood cell wall, where it may promote the degradation process. Also, reaction mechanisms between Cu(II), 2,3-DHBA and H_2O_2 have been proposed which provide at least partial explanations for the H_2O_2 cycle, and the mechanism for non-enzymatic, chelator–mediated Fenton reactions in brown rot wood decay processes.

Future research in this area should explore cyclic voltammetry analyses of Cu(II) and ligands secreted by fungi, such as 2,5-DMHQ or 2,5-DMBQ in the absence or presence of H_2O_2 under a range of acidic conditions. Cyclic voltammetry experiments should also be conducted with Fe(III), oxalic acid and ligands secreted by fungi, to gain insight into the mechanism and kinetics of the relevant redox reactions in wood decay processes.

BIBLIOGRAPHY

1. Campbell, W.G., *The biological decomposition of wood.*, in *Wood Chemistry*, Wise, L.E. and Jahn, E.C., Editors. 1952, Rheinhold Pub. Corp.: New York. p. 1061-1116.

2. Schmidt, C.J., Whitten, B.K., and Nicholas, D.D., *A proposed role for oxalic acid in nonenzymatic wood decay by brown-rot fungi.* Proc. Am. Wood-preserv. Assoc., 1981. **77**: p. 157-164.

3. Koenigs, J.W., *Production of extracellular hydrogen peroxide by wood-rotting fungi.* Phytopathology, 1972. **62**: p. 100-110.

4. Koenigs, J.W., *Hydrogen peroxide and iron: A microbial cellulolytic system?* Biotechnology Bioengineering Symposium, 1975. **5**: p. 151-159.

5. Goodell, B., Jellison, J., Liu, J., Daniel, G., Paszczynski, A., Fekete, F., Krishnamurthy, S., Jun, L., and Xu, G., *Low molecular weight chelators and phenolic compounds isolated from wood decay fungi and their role in the fungal biodegradation of wood.* J. Biotechnol., 1997. **53**: p. 133-162.

6. Paszczynski, A., Crawford, R., Funk, D., and Goodell, B., *De Novo synthesis of 4,5-dimethoxycatechol and 2,5-dimethoxyhydroquinone by the brown rot fungus Gloeophyllum trabeum.* Appl. and Environ. Microbiology, 1999. **65**(2): p. 674-679.

7. Kerem, Z., Jensen, K.A., and Hammel, K.E., *Biodegradative mechanism of the brown rot basidiomycete Gloeophyllum trabeum: evidence for an extracellular hydroquinone-driven fenton reaction.* FEBS Letters, 1999. **446**: p. 49-54.

8. Jensen, J.K.A., Houtman, C.J., Ryan, Z.C., and Hammel, K.E., *Pathways for extracellular Fenton chemistry in the brown rot basidiomycete Gloeophyllum trabeum.* Appl. and Environ. Microbiology, 2001. **67**(6): p. 2705-2711.

9. Illman, B.S. and Highley, T.L., *Decomposition of wood by brown-rot fungi.*, in *Biodeterioration Research 2*, O'Rear, C.E. and Llewellyn, G.C., Editors. 1989, Plenum Press: New York. p. 465-484.

10. Halliwell, G., *Catalytic decomposition of cellulose substrates.* Biochemistry Journal., 1965. **95**: p. 35-40.

11. Henry, W.P., *Non-Enzymatic Iron, Manganese, and Copper Chemistry of Potential Importance in Wood Decay*, in *Wood Deterioration and Preservation: Advances in Our Changing World*, Goodell, B., Nicholas, D.D., and Schultz, T.P., Editors. 2003, American Chemistry Society: Washington, DC. p. 175-195.

12. Kirk, T.K., *Effects of a brown-rot fungus Lenzites frabea: on lignin in spruce wood.* Holzforsch., 1975. **29**(3): p. 99-107.

13. Reese, E.T., Siu, R.G.H., and Levinson, H.S., *The biological degradation of soluble cellulose derivatives and its relationship to the mechanism of cellulose hydrolysis.* J. Bacteriol., 1950. **59**: p. 485-497.

14. Cowling, E.B., *Comparative biochemistry of the decay of sweetgum sapwood by white-rot and brown-rot fungi.* Tech. Bull. 1258 USDA Washington, DC, 1961: p. 79.

15. Kim, Y.S., Goodell, B., and Jellison, J., *Immunogold labeling of extracellular metabolites from the white-rot fungus Trametes versicolor.* Holzforsch., 1993. **47**: p. 25-28.

16. Green III, F. and Highley, T., *Mechanism of Brown-rot Decay: Paradigm or Paradox.* Inter. Biodeter. Biodegrad., 1997. **39**(2-3): p. 113-124.

17. Haber, F. and Weiss, J., *The catalytic decomposition of hydrogen peroxide by iron salts.* Proc. R. Soc. Lond. (A), 1934. **147**: p. 332-351.

18. Highley, T., *Degradation of cellulose by Poria placenta in the presence of compounds that affect hydrogen peroxide.* Mater. Org., 1980. **15**: p. 81-90.

19. Hyde, S.M. and Wood, P.M., *A mechanism for production of hydroxyl radicals by the brown-rot fungus Coniophora puteana: Fe(III) reduction by cellobiose dehydrogenase and Fe(II) oxidation at a distance from the hyphae.* Microbiology, 1997. **143**: p. 259-266.

20. Enoki, A., Hirano, T., and Tanaka, H., *Extracellular substance from brown-rot basidiomycete G. trabeum that produces and reduces hydrogen peroxide.* Mater. Org., 1992. **27**: p. 247-261.

21. Enoki, A., Itakura, S., and Tanaka, H., *The involvement of extracellular substances for reducing molecular oxygen to hydroxyl radical and ferric iron to ferrous iron in wood degradation by wood decay fungi.* J. Biotechnol., 1997. **53**: p. 265-272.

22. Shimada, M., Akamtsu, Y., Tokimatsu, T., Mii, K., and Hattori, T., *Possible biochemical roles of oxalic acid as a low molecular weight compound involved in brown-rot and white-rot wood decays.* J. Biotechnol., 1997. **53**: p. 103-113.

23. Sulzberger, B. and Laubsher, H., *Reactivity of various types of iron(III) (hydr)oxides towards light-induced dissolution.* Mar. Chem., 1995. **50**: p. 103-115.

24. Zepp, R.G., Faust, B.C., and Hoigne, J., *Hydroxyl radical formation in aqueous reactions (pH 3-8) of iron(II) with hydrogen peroxide: The photo-Fenton reaction.* Environ. Sci. Technol., 1992. **26**: p. 313-319.

25. Hammel, K.E., Kapich, A.N., Jensen Jr., K.A., and Ryan, Z.C., *Reactive oxygen species as agents of wood decay by fungi.* Enzyme and Microbial Technology, 2002. **30**: p. 445-453.

26. Wang, W. and Gao, P.J., *A peptide-mediated and hydroxyl radical HO· -involved oxidative degradation of cellulose by brown-rot fungi.* Biodegradation, 2002. **13**: p. 383-394.

27. Wang, W. and Gao, P.J., *Function and mechanism of a low-molecular-weight peptide produced by Gloeophyllum trabeum in biodegradation of cellulose.* J. Biotechnol., 2003. **101**: p. 119-130.

28. Fekete, F.A., Chandhoke, V., and Jellison, J., *Iron-binding compounds produced by wood-decaying basidionmycetes.* Appl. and Environ. Microbiology, 1989. **55**: p. 2720-2722.

29. Jellison, J., Chanhoke, V., Goodell, B., and Fekete, F., *The isolation and immunolocalization of iron-binding compounds produced by Gloeophyllum trabeum.* Appl. and Environ. Microbiology, 1991. **35**: p. 805-809.

30. Jellison, J., Chanhoke, V., Goodell, B., and Fekete, F. *The action of siderophores isolated from Gloeophyllum trabeum on the structure and crystallinity of cellulose.* in *International Research group on wood preservation series. Box 5607, S-114 86.* 1991. Stockholm, Sweden. p. 1479.

31. Lu, J., Goodell, B., Liu, J., Enoki, A., Jellison, J., Tanaka, H., and Fekete, F. *The role of oxygen and oxygen radicals in the one-electron oxidative reactions mediated by low-molecular weight chelators isolated from Gloeophyllum trabeum.* in *International working group on wood preservation series. Box 5607, S-114 86.* 1994. Stockholm, Sweden. p. 1086.

32. Jellison, J., Connolly, J., Goodell, B., Doyle, B., Illman, B., Fekete, F., and Ostrofsky, A., *The role of cations in the biodegradation of wood by the brown rot fungi.* Inter. Biodeter. Biodegrad., 1997. **39**(2-3): p. 165-179.

33. Kremer, S.M. and Wood, P.M., *Production of Fenton's reagent by cellobiose oxidase from cellulolytic cultures of Phanerochaete chiysosporium.* Eur. J. Biochem., 1992. **208**: p. 807-814.

34. Xu, G. and Goodell, B., *Mechanisms of wood degradation by brown-rot fungi: chelator-mediated cellulose degradation and binding of iron by cellulose.* J. Biotechnol., 2001. **87**: p. 43-57.

35. Jensen, J.K.A., Ryan, Z.C., Wymelenberg, A.V., Cullen, D., and Hammel, K.E., *An NADH: Quinone Oxidoreductase active during biodegradation by the brown-rot basidiomycete Gloeophyllum trabeum.* Appl. and Environ. Microbiology, 2002. **68**(6): p. 2699-2703.

36. Goodell, B., Qian, Y., Jellison, J., Richard, M., and Qi, W., *Lignocellulose oxidation by low molecular weight metal-binding compounds isolated from wood degrading fungi: A comparison of brown rot and white rot systems and the potential application of chelator-mediated Fenton reactions.*, in *Progress in*

Biotechnology 21: Biotechnology in the pulp and paper industry., Viikari, L. and Lantto, R., Editors. 2002, ELSEVIER: Fin-02044 VTT, Finland. p. 37-48.

37. Qian, Y., Goodell, B., and Felix, C.C., *The effect of hydroxyl radical generation on free-radical activation of TMP fibers.* unpublished, 2003.

38. Sigg, L. and Xue, H., *Metal speciation: concepts, analysis and effects.*, in *Chemistry of Aquatic Systems: Local and Global Perspectives,*, Bidoglio, G. and Stumm, W., Editors. 1994, Brussels and Luxembourg: Netherlands. p. 153-181.

39. Sunda, W.G., *Trace metal/phytoplankton interactions in the sea*, in *Chemistry of Aquatic Systems: Local and Global Perspectives*, Bidioglio, G. and Stumm, W., Editors. 1994, Brussels and Luxembourg: Netherlands. p. 213-247.

40. Sunda, W.G. and Ferguson, R.L. *Sensitivity of natural bacterial communities to additions of copper and to cupric ion activity: A bioassay of copper complexation in seawater.* in *NATO Conf. Ser. 4.* 1983. p. 871-891.

41. Florence, T.M., *Electrochemical approaches to trace element speciation in waters-a review.* Analyst., 1986. **111**: p. 489-505.

42. Chau, Y.K., Gachter, R., and Lum-Shu-Chan, K., *Determination of the apparent complexation capacity of lake water.* J. Fish. Res. Board Can., 1974. **31**: p. 1515-1519.

43. Goncalves, M.L.S., Sigg, L., and Stumm, W., *Voltammetric methods for distinguishing between dissolved and particulate metal ion concentrations in the presence of hydrous oxides. A case study on lead(II).* Environ. Sci. Technol., 1986. **19**: p. 141-146.

44. Coale, K.H. and Bruland, K.W., *Copper complexation in the northeast Pacific.* Limnol. Oceanogr., 1988. **33**: p. 1084-1101.

45. Scarano, G., Gramanti, E., and Zirino, A., *Determination of copper complexation in sea water by a ligand competition technique with voltammetric measurement of the labile metal fraction.* Anal. Chim. Acta., 1992. **264**: p. 153-162.

46. Berg, V.d., *Determination of the complexing capacity and conditional stability constants of complexes of copper(II) with natural organic ligands in seawater by cathodic stripping voltammetry of copper-catechol complex ions.* Mar. Chem., 1984. **15**: p. 1-18.

47. Berg, V.d., Constant, M.G., and Nimmo, M., *Effects of the detection window on the determination of organic copper speciation in estuarine waters.* Anal. Chim. Acta., 1990. **232**: p. 149-159.

48. Xue, H. and Sigg, L., *Free cupric ion concentration and Cu(II) speciation in a eutrophic lake.* Limnol. Oceanogr., 1993. **38**: p. 1200-1213.

49. Xue, H. and Sunda, W.G., *Comparison of [Cu^{2+}] measurements in lake water determined by ligand exchange and cathodic stripping voltammetry and by ion-selective electrode.* Environ. Sci. Technol., 1997. **31**: p. 1902-1909.

50. Wu, J. and Luther III, G.W., *Complexation of Fe(III) by natural organic ligands in the Northwest Atlantic ocean by a competitive ligand equilibration method and a kinetic approach.* Mar. Chem., 1995. **50**: p. 159-177.

51. Muller, F.L.L., *Interactions of copper, lead and cadmium with the dissolved, colloidal and particulate components of estuarine and coastal waters.* Mar. Chem., 1996. **52**: p. 245-268.

52. Gledhill, M., Constant, M.G., and Berg, V.d., *Measurement of the redox speciation of iron in seawater by catalytic cathodic stripping voltammetry.* Mar. Chem., 1995. **50**: p. 51-61.

53. Voelker, B.M. and Kogut, M.B., *Interpretation of metal speciation data in coastal waters: the effects of humic substances on copper binding as a test case.* Mar. Chem., 2001. **74**: p. 303-318.

54. Kogut, M.B. and Voelker, B.M., *Strong copper-binding behavior of terrestrial humic substances in seawater.* Environ. Sci. Technol., 2001. **35**: p. 1149-1156.

55. Lewis, B.L., Holt, P.D., Taylor, S.W., Wilhelm, S.W., Trick, C.G., Butler, A., and Luther III, G.W., *Voltammetric estimation of iron(III) thermodynamic stability constants for catecholate siderophores isolated from marine bacteria and cyanobacteria.* Mar. Chem., 1995. **50**: p. 179-188.

56. Wang, J., *Analytical Electrochemistry.* 2000, New York: Wiley-VCH. p. 29.

57. Http://www.bath.ac.uk/~chsacf/solartron/electro/html/cv.htm.

58. Nicholson, R.S. and Shain, I., *Theory of Stationary Electrode Polarograghy: Single Scan and Cyclic Methods Applied to Reversible, Irreversible, and Kinetics Systems.* Anal. Chem., 1964. **36**(4): p. 706-723.

59. Hatzipanayioti, D., Karaliota, A., Kamariotaki, M., and Veneris, A., *Electrochemical and spectroscopic studies of 2,3-dihydroxy-benzioc acid, its oxidation products and their interaction with manganese(II), in dimethyl sulfoxide solutions.* Transition Metal Chemistry, 1998. **23**(4): p. 407-416.

60. Bodini, M., Osorio, C.M., and Valle, A.D., *Redox chemistry of 3,4-dihydroxy-2-benzoic acid, its oxidation products and their interaction with Manganese(II) and Manganese(III).* Pergamon, 1995. **14**(20-21): p. 2933-2936.

61. Yokoi, K., Berg, V.d., and Constant, M.G., *The determination of iron in sea water using catalytic cathodic stripping voltammetry.* Electroanalysis, 1992. **4**: p. 65-69.

62. Westall, J.C., *MICROQL, A Chemical Equilibrium Program in Basic.* 1986, Oregon State University: Corvallis, OR.

63. Herbelin, A. and Westall, J., *FITEQL3. Report 94-01.* 1994, Department of Chemistry, Oregon State University: Corvallis, Oregon.

64. Motekaitis, R.J., *NIST Critically Selected Stability Constants of Metal Complexes Database.* 2001, U.S. Department of Commerce: Gaithersburg, MD.

65. Stumm, W. and Morgan, J.J., *Aquatic Chemistry.* 3rd ed. 1996, New York: John Wiley & Sons. p. 325-336.

66. Xue, H. and Sigg, L., *Cadmium speciation and complexation by natural organic ligands in fresh water.* Anal. Chim. Acta., 1998. **363**(2-3): p. 249-259.

67. Filley, T.R., Cody, G.D., Goodell, B., Jellison, J., Noser, C., and Ostrofsky, A., *Lignin demethylation and polysaccharide decomposition in spruce sapwood degraded by brown rot fungi.* Organic Geochemistry, 2002. **33**: p. 111-124.

68. Moffett, J.W., Zika, R.G., and Petasne, R.G., *Evaluation of bathocuproine for the spectrophotometric determination of Copper(I) in Copper redox studies with applications in studies of natural waters.* Anal. Chim. Acta., 1985. **175**: p. 171-179.

69. Gili, P., Reyes, M.M., and Zaza, P.M., *Complexes of Mn(II) and Mn(III) with the Schiff base N-[2-(3-ethylindole)]pyridoxaldimine. Electrochemical study of these and related Ni(II) and Cu(II) complexes.* Inorg. Chim. Acta., 1997. **255**(2): p. 279-288.

70. Bard, A.J. and Faulkner, L.R., *Electrochemical Methods: fundamentals and applications*. 2 ed. 2001, New York: John Wiley & Sons, Inc. p. 226-255.

71. Martell, A.E. and Smith, R.M., *Critical Stability Constants*. Vol. 5. 1982, New York: Plenum Press. p. 345.

72. Kamau, P. and Jordan, R.B., *Kinetic Study of the Oxidation of Catechol by Aqueous Copper(II).* Inorg. Chem., 2002. **41**: p. 3076-3083.

73. Xu, J. and Jordan, R.B., *Kinetics and mechanism of the oxidation of 2,3-dihydroxybenzoic acid by iron(III).* Inorg. Chem., 1988. **27**: p. 4563-4566.

74. Qian, Y., Goodell, B., and Felix, C.C., *The effect of low molecular weight chelators on iron chelation and free radical generation as studied by ESR measurement.* Chemosphere, 2002. **48**: p. 21-28.

75. Sedlak, D.L. and Hoigne, J., *The role of copper and oxalate in the redox cycling of iron in atmospheric waters.* Atmospheric Environment, 1993. **27A**(14): p. 2173-2185.

76. Paczesniak, T. and Sobkowiak, A., *The influence of solvent on the reaction between iron(II), (III) and hydrogen peroxide.* Journal of Molecular Catalysis A: Chemical, 2003. **194**: p. 1-11.

BIOGRAPHY OF THE AUTHOR

Ran Liu was born in Fangzhen, Heilongjiang Province in China on August 11th, 1975. She grew up in Weifang, Shangdong province and graduated from The First Weifang High School in 1993. She attended Harbin Engineering University and graduated in 1997 with a Bachelor's degree in Electrochemical Engineering. She continued her graduate study in Beijing University of Chemical and Technology and graduated in 2000 with a Master's degree in Materials Science and Engineering. In fall 2001, Ran entered the Civil and Environmental Engineering graduate program at The University of Maine.

After receiving her degree, Ran will be joining the Civil and Environmental Engineering program at Carnegie Mellon University, to continue studying for a Ph.D. degree. Ran is a candidate for the Master of Science degree in Civil Engineering from The University of Maine in August, 2003.